

A Possible Mass Ratio and Spin-Orbit Misalignment Correlation for Mergers of Binary Black Holes in Nuclear Star Clusters

YUBO SU ¹

¹*Department of Astrophysical Sciences, Princeton University, Princeton, NJ 08544, USA*

(Received XXXX; Revised YYYY; Accepted ZZZZ)

Submitted to ApJ

ABSTRACT

Despite a decade’s worth of gravitational wave observation, the origin of the binary black hole (BBH) mergers detected by the LIGO-VIRGO-Kagra (LVK) collaboration remains an open question. Towards assessing the feasibility and prevalence of the many proposed BBH formation channels, the spin properties of the merging black holes (BHs) hold significant promise, particularly their orientations. The combined trends of a moderate preferential alignment of BH spins with their orbit normals and an apparent correlation of BBH effective spin parameters χ_{eff} with their mass ratios seem to favor hydrodynamical BBH formation mechanisms over purely dynamical ones, as they introduce a preferred orientation to the system. However, such processes are filled with physical and modeling uncertainties. In this paper, we highlight a dynamical route to easily characterizable spin evolution that results in analytically-predictable spin distributions. We show that, when a stellar binary forms a BBH through two phases of stable mass transfer, and the BBH is subsequently driven to merger by the gravitational perturbation of a distant massive object (such as a supermassive black hole), the resulting spin-orbit misalignment angles are anti-correlated with the binary mass ratio. While the mechanism as proposed only operates in a somewhat narrow region of parameter space, it also predicts significantly tighter correlations than are seen in the LVK systems. We discuss avenues for future work that may significantly expand the parameter space of our mechanism while still remaining broadly consistent with observations.

1. INTRODUCTION

As of today, partway through the fourth observing run of the LIGO-VIRGO-Kagra (LVK) Collaboration, a total of ~ 150 compact object mergers has been detected (Abbott et al. 2023; Callister 2024), the large majority of which are merging binary black holes (BBHs). Many properties of these systems can be discerned from their gravitational wave (GW) waveform, such as the binaries’ component masses, mass ratios, and spin properties. In principle, these properties should carry information about the formation mechanism(s) of BBHs. In practice, such an inference has proven difficult despite extensive efforts. Broadly, three classes of formation channels can be identified. The first is the class of isolated BBH formation, where an isolated stellar binary evolves into a

merging BBH in isolation from any additional perturbations (e.g., Lipunov et al. 1997; Podsiadlowski et al. 2003; Belczynski et al. 2010; Dominik et al. 2012; Belczynski et al. 2016; Mandel & De Mink 2016; De Mink & Mandel 2016; Marchant et al. 2016; Belczynski et al. 2020; Riley et al. 2021; Fragos et al. 2023; Marchant & Bodensteiner 2024; Andrews et al. 2024). The second is the class of hydrodynamically-assisted BBH mergers, typically in the disks of active galactic nuclei (AGN), where the BBH is formed and/or driven towards merger due to interactions with the dense surrounding gas (e.g. McKernan et al. 2012; Stone et al. 2017; Leigh et al. 2018; Secunda et al. 2019; Tagawa et al. 2020; Li et al. 2021; Li & Lai 2022; Li et al. 2022; Samsing et al. 2022; McKernan et al. 2022; Rowan et al. 2023; Whitehead et al. 2024; McKernan et al. 2024). The third is the class of dynamically-assisted BBH mergers, where an initially wide binary is induced to merge via interactions with either a few (e.g., Miller & Hamilton 2002; Wen 2003;

Antonini & Perets 2012a; Antonini et al. 2014; Silsbee & Tremaine 2017; Liu & Lai 2017, 2018; Randall & Xianyu 2018; Hoang et al. 2018; Fragione & Loeb 2019; Liu & Lai 2019; Liu et al. 2019a,b; Liu & Lai 2020; Su et al. 2021a; Michaely & Perets 2020; Liu & Lai 2021; Su et al. 2021b; Martinez et al. 2022; Grishin & Perets 2022; Su et al. 2024) or many (e.g. Portegies Zwart & McMillan 2000; O’leary et al. 2006; Miller & Lauburg 2009; Banerjee et al. 2010; Downing et al. 2010; Ziosi et al. 2014; Rodriguez et al. 2015; Antonini & Rasio 2016; Samsing & Ramirez-Ruiz 2017; Samsing & D’Orazio 2018; Rodriguez et al. 2018; Gondán et al. 2018; Barber & Antonini 2024; Bruel et al. 2024) bodies, including many studies on BBH mergers in nuclear star clusters (e.g. Antonini et al. 2010; Antonini & Perets 2012b; Leigh et al. 2016, 2018; Hoang et al. 2018; Fragione et al. 2019; Chattopadhyay et al. 2023; see Arca Sedda et al. 2023 for a review). The question of which of these channels contributes what fraction of the observed BBH mergers remains an open question (Zevin et al. 2021; Costa et al. 2023), and there is an ever-expanding effort to understand both the predicted properties of BBHs formed via each formation mechanism and the observed properties of the merging systems in the LVK data.

One strong discriminant among these channels is the spin orientation of the merging BBHs. From the GW waveform of a merging BBH, two constraints can be inferred on the spins of the component black holes (BHs). First, the most well-measured combination of spin properties is the parameter

$$\chi_{\text{eff}} \equiv \frac{m_1 \chi_1 \cos \theta_1 + m_2 \chi_2 \cos \theta_2}{m_1 + m_2}, \quad (1)$$

where m_i is the mass of the i th component, χ_i is its spin magnitude (where 1 corresponds to a maximally rotating BH), and θ_i is the angle between the spin of the i th BH and the total orbital angular momentum of the BBH. Second, the relativistic precession of the BBH’s orbital plane constrains the in-plane component of the component spins via the phenomenological parameter (Schmidt et al. 2015)

$$\chi_p \equiv \max \left[\chi_1 \sin \theta_1, \left(\frac{3 + 4q}{4 + 3q} \right) q \chi_2 \sin \theta_2 \right], \quad (2)$$

where $q = m_2/m_1 < 1$ is the mass ratio of the BHs. As of the LVK O3b data release, the population-level statistics on these two parameters are as follows: the χ_{eff} distribution has mean $0.06^{+0.04}_{-0.05}$ and extends to negative values, while the χ_p distribution is broadly centered at zero with standard deviation $0.16^{+0.15}_{-0.08}$ (Abbott et al. 2023). In terms of physical parameters, the BHs seen by LVK are moderately spinning ($\langle \chi_i \rangle \sim 0.2$) and

have broadly distributed spin-orbit misalignment angles (θ_i moderately favors alignment, but at least some BHs have $\theta_i > 90^\circ$; Abbott et al. 2023; Callister & Farr 2024). Furthermore, there is evidence for an anti-correlation between χ_{eff} and q , such that lower-mass-ratio systems have larger χ_{eff} (Callister et al. 2021)—this trend has grown stronger with the O3b data release (Abbott et al. 2023). Taken together, these properties of the LVK sample suggest that at least some BBHs form through channels that preferentially yield aligned spins.

The natural next question is: which BBH formation channels satisfy this constraint? Isolated evolution is manifestly capable of producing BBHs with aligned spins, and more recent work suggests that sufficient spin-orbit misalignment can also be generated via isolated evolution to ensure consistency with the LVK data (e.g. Steinle & Kesden 2021; Banerjee & Olejak 2024). BBH formation in AGN disks can also introduce a preferred orientation for the spins and orbit of the BBH, leading to preferential spin-orbit alignment (e.g. Wang et al. 2021; Cook et al. 2024). However, studies generally find that BBHs experiencing dynamically violent evolution result in χ_{eff} distributions distributed symmetrically and broadly about a peak at 0 (e.g. Antonini et al. 2017; Liu & Lai 2018; Rodriguez et al. 2018; Liu et al. 2019a; Yu et al. 2020; Fragione & Kocsis 2020; Su et al. 2021a; Arca Sedda et al. 2023). Such a distribution arises when the BH spins are isotropically oriented, which results in a uniform distribution for $\cos \theta_i \in [-1, 1]$ (Eq. 1) and a wedge distribution for χ_{eff} . As such, at first glance, it would appear that dynamically-induced BBH mergers are disfavored by the LVK constraints on the spin properties of merging BBHs.

This is not necessarily the case. Within the class of dynamically-driven BBH merger channels, those involving just a single tertiary companion (“tertiary-induced mergers”) can produce sharp features in the distribution of BH spin orientations under the right conditions—this was first pointed out in the numerical work as a “90° attractor” of spin-orbit misalignment (Liu & Lai 2018; Yu et al. 2020; Su et al. 2021a). Subsequent work showed that this attractor arises due to a dynamical invariant linking the initial and final spin orientations of the BHs (Su et al. 2021a). Importantly, this process prefers specific spin orientations despite being a dynamically-driven BBH merger channel.

In this work, we show that tertiary-induced mergers, specifically driven by a supermassive BH (SMBH) tertiary, may be able to reproduce many of the features of the spin distribution observed by LVK. Notably, the resulting spin-orbit misalignment angles are preferentially prograde and may be anti-correlated with the mass ratio

of the BBH. In Section 2, we review the orbital and spin evolution of a BBH in the tertiary-induced merger channel, including the dynamical invariant that gives rise to the spin attractor. In Section 3, we discuss our semi-analytical model of the binary stellar evolution giving rise to the BBHs we consider. In Section 4, we show that the combined stellar and dynamical evolution can give rise to unexpected correlations in the spin properties of merging BBHs. In Section 5, we discuss the feasibility and efficiency of our mechanism when taking into account the nuclear star cluster that typically surrounds SMBHs. We summarize and discuss in Section 6.

2. TERTIARY-INDUCED MERGERS AND SPIN DYNAMICS

In a tertiary-induced merger channel, two black holes orbit each other on a compact orbit while they together are in a distant orbit with a tertiary companion. The orbit of the two inner black holes, with masses m_1 and m_2 , is described by the Keplerian orbital elements a_{in} , e_{in} , I_{in} , ω_{in} , and Ω_{in} , corresponding to the binary’s semi-major axis, eccentricity, inclination, argument of pericenter, and longitude of the ascending node respectively. The outer orbit, of the two black holes about the tertiary with mass m_3 , is analogously described by a_{out} , e_{out} , I_{out} , ω_{out} , and Ω_{out} . The reference frame is oriented with the total angular momentum pointed along the polar axis (which is nearly equal to the outer orbit’s angular momentum). Finally, call I the mutual inclination between the two orbits.

In absence of an outer companion, the inner binary will merge due to emission of GWs on a characteristic timescale (assuming a circular orbit, e.g. Liu & Lai 2018) of

$$T_{\text{m},0} \equiv \frac{5c^5 a_{\text{in}}^4}{256G^3 m_{12}^2 \mu_{\text{in}}} \simeq 10^{10} \left(\frac{m_{12}}{100M_{\odot}} \right)^{-2} \left(\frac{\mu_{\text{in}}}{25M_{\odot}} \right)^{-1} \left(\frac{a_{\text{in}}}{0.3 \text{ AU}} \right)^4 \text{ yrs}, \quad (3)$$

where $m_{12} = m_1 + m_2$ and $\mu_{\text{in}} = m_1 m_2 / m_{12}$ is the reduced mass. Thus, binaries with $a_{\text{in}} \gtrsim 0.3 \text{ AU}$ will take longer than a Hubble time (10^{10} yrs) to merge in isolation. Such binaries can nevertheless be induced to merge due to gravitational interactions with their tertiary companion—such mergers are termed “tertiary-induced mergers”. In this section, we review the orbital and spin evolution of the inner black holes (m_1 and m_2) in a tertiary-induced merger.

2.1. Orbital Evolution: von Zeipel-Lidov-Kozai Effect

The tertiary companion can accelerate the merger of the inner binary by exciting its eccentricity due to the von Zeipel-Lidov-Kozai (ZLK, von Zeipel 1910; Lidov 1962; Kozai 1962) effect: when the inner and outer orbits are misaligned (when the mutual inclination I is between $\sim 39^\circ$ and $\sim 141^\circ$), the eccentricity and inclination of the inner binary will oscillate. As $I \rightarrow 90^\circ$, the maximum of these eccentricity oscillations can approach near-unity, resulting in efficient GW radiation at each pericenter passage (e.g. Liu et al. 2015a; Naoz 2016).

The orbital evolution of the two binaries is due to a combination of Newtonian and General Relativistic (GR) effects. We implement the Newtonian evolution of the inner and outer binaries by expanding their mutual gravitational interaction to the octupole order, double-averaging (over both the inner and outer orbits), and including the leading-order corrections to the double-averaged approximation via “Brown’s Hamiltonian” (as given by Eq. 64 of Tremaine 2023). We adopt the common vectorial formulation, where the inner and outer orbits are described by their orbital angular momentum and eccentricity vectors (e.g. Liu & Lai 2018; Su et al. 2021a)

$$\mathbf{L}_{\text{in}} = L_{\text{in}} \mathbf{j}_{\text{in}} = \mu_{\text{in}} \sqrt{G m_{12} a_{\text{in}}} \mathbf{j}_{\text{in}}, \quad (4)$$

$$\mathbf{e}_{\text{in}} = e_{\text{in}} \hat{\mathbf{e}}_{\text{in}}, \quad (5)$$

$$\mathbf{L}_{\text{out}} = \mu_{\text{out}} \sqrt{G m_{123} a_{\text{out}}} \mathbf{j}_{\text{out}}, \quad (6)$$

$$\mathbf{e}_{\text{out}} = e_{\text{out}} \hat{\mathbf{e}}_{\text{out}}. \quad (7)$$

Here, $\mu_{\text{out}} \equiv m_{12} m_3 / m_{123}$ and $m_{123} = m_{12} + m_3$, and $\mathbf{j}_{\text{in}} \equiv j_{\text{in}} \hat{\mathbf{j}}_{\text{in}}$ where $j_{\text{in}}^2 \equiv 1 - e_{\text{in}}^2$ (and analogously for j_{out}).

Then, the interaction potential between the two orbits is given by (Liu & Lai 2018; Tremaine 2023; Grishin 2024)

$$\Phi = \Phi_{\text{quad}} + \Phi_{\text{oct}} + \Phi_{\text{B}}, \quad (8)$$

$$\Phi_{\text{quad}} = \Phi_0 \left[1 - 6e_{\text{in}}^2 - 3(\mathbf{j}_{\text{in}} \cdot \hat{\mathbf{j}}_{\text{out}})^2 + 15(\mathbf{e}_{\text{in}} \cdot \hat{\mathbf{j}}_{\text{out}})^2 \right], \quad (9)$$

$$\begin{aligned} \Phi_{\text{oct}} = & \frac{15}{8} \epsilon_{\text{oct}} \Phi_0 \left[(\mathbf{e}_{\text{in}} \cdot \hat{\mathbf{e}}_{\text{out}}) \right. \\ & \times \left(8e_{\text{in}}^2 - 1 + 5(\mathbf{j}_{\text{in}} \cdot \hat{\mathbf{j}}_{\text{out}})^2 - 35(\mathbf{e}_{\text{in}} \cdot \hat{\mathbf{j}}_{\text{out}})^2 \right) \\ & \left. + 10(\mathbf{e}_{\text{in}} \cdot \hat{\mathbf{j}}_{\text{out}})(\mathbf{j}_{\text{in}} \cdot \hat{\mathbf{e}}_{\text{out}})(\mathbf{j}_{\text{in}} \cdot \hat{\mathbf{j}}_{\text{out}}) \right], \quad (10) \end{aligned}$$

$$\begin{aligned} \Phi_{\text{B}} = & \frac{3(3 + 2e_{\text{out}}^2)}{8} \epsilon_{\text{SA}} \Phi_0 (\mathbf{j}_{\text{in}} \cdot \hat{\mathbf{j}}_{\text{out}}) \\ & \times \left(24e_{\text{in}}^2 - 15(\mathbf{e}_{\text{in}} \cdot \hat{\mathbf{j}}_{\text{out}})^2 - (\mathbf{j}_{\text{in}} \cdot \hat{\mathbf{j}}_{\text{out}})^2 + 1 \right). \quad (11) \end{aligned}$$

We have defined the standard quantities (e.g. Liu et al. 2015a; Grishin 2024)

$$\Phi_0 = \frac{Gm_1m_2m_3a_{\text{in}}^2}{8m_{12}a_{\text{out}}^3j_{\text{out}}^3}, \quad (12)$$

$$\epsilon_{\text{oct}} \equiv \frac{m_1 - m_2}{m_{12}} \frac{a_{\text{in}}}{a_{\text{out}}} \frac{e_{\text{out}}}{1 - e_{\text{out}}^2}, \quad (13)$$

$$\epsilon_{\text{SA}} \equiv \left(\frac{m_3^2}{m_{12}m_{123}} \right)^{1/2} \left(\frac{a_{\text{in}}}{a_{\text{out}}j_{\text{out}}^2} \right)^{3/2}. \quad (14)$$

The Newtonian evolution of the two binaries can then be derived, at our adopted level of approximation, from the Milankovitch equations (e.g. Tremaine et al. 2009; Liu et al. 2015a)

$$\left. \frac{d\mathbf{L}_{\text{in}}}{dt} \right|_{\text{N}} = - [\mathbf{j}_{\text{in}} \times \nabla_{\mathbf{j}_{\text{in}}} \Phi + \mathbf{e}_{\text{in}} \times \nabla_{\mathbf{e}_{\text{in}}} \Phi], \quad (15)$$

$$\left. \frac{d\mathbf{e}_{\text{in}}}{dt} \right|_{\text{N}} = - \frac{1}{L_{\text{in}}} [\mathbf{j}_{\text{in}} \times \nabla_{\mathbf{e}_{\text{in}}} \Phi + \mathbf{e}_{\text{in}} \times \nabla_{\mathbf{j}_{\text{in}}} \Phi], \quad (16)$$

$$\left. \frac{d\mathbf{L}_{\text{out}}}{dt} \right|_{\text{N}} = - [\mathbf{j}_{\text{out}} \times \nabla_{\mathbf{j}_{\text{out}}} \Phi + \mathbf{e}_{\text{out}} \times \nabla_{\mathbf{e}_{\text{in}}} \Phi], \quad (17)$$

$$\left. \frac{d\mathbf{e}_{\text{out}}}{dt} \right|_{\text{N}} = - \frac{1}{L_{\text{out}}} [\mathbf{j}_{\text{out}} \times \nabla_{\mathbf{e}_{\text{out}}} \Phi + \mathbf{e}_{\text{out}} \times \nabla_{\mathbf{j}_{\text{out}}} \Phi]. \quad (18)$$

Here, the gradients denote $\nabla_{\mathbf{v}} \Phi \equiv \sum_i \partial \Phi / \partial v_i \hat{\mathbf{e}}_i$, where $\hat{\mathbf{e}}_i$ is the i th basis vector. We implement these gradients using the computer algebra system `sympy` (Meurer et al. 2017).

In addition to the Newtonian orbital evolution, we consider two general relativistic effects. The first is GR pericenter precession, a first-order post-Newtonian (1-PN) effect (e.g. Liu & Lai 2018)

$$\left. \frac{d\mathbf{e}_{\text{in}}}{dt} \right|_{\text{GR}} = \Omega_{\text{GR}} \mathbf{L}_{\text{in}} \times \hat{\mathbf{e}}_{\text{in}}, \quad (19)$$

$$\Omega_{\text{GR}} = \frac{3Gm_{12}}{c^2 a_{\text{in}} j_{\text{in}}^2} n_{\text{in}}, \quad (20)$$

where $n_{\text{in}} = \sqrt{Gm_{12}/a_{\text{in}}^3}$ is the mean motion of the inner binary. The second is GW emission, a 2.5-PN effect (Peters 1964)

$$\left. \frac{d\mathbf{L}_{\text{in}}}{dt} \right|_{\text{GW}} = - \frac{32}{5} \frac{G^3 \mu_{\text{in}} m_{12}^2}{c^5 a_{\text{in}}^4 j_{\text{in}}^5} \left(1 + \frac{7e_{\text{in}}^2}{8} \right) \mathbf{L}_{\text{in}}, \quad (21)$$

$$\left. \frac{d\mathbf{e}_{\text{in}}}{dt} \right|_{\text{GW}} = - \frac{304}{15} \frac{G^3 \mu_{\text{in}} m_{12}^2}{c^5 a_{\text{in}}^4 j_{\text{in}}^5} \left(1 + \frac{121e_{\text{in}}^2}{304} \right) \mathbf{e}_{\text{in}}. \quad (22)$$

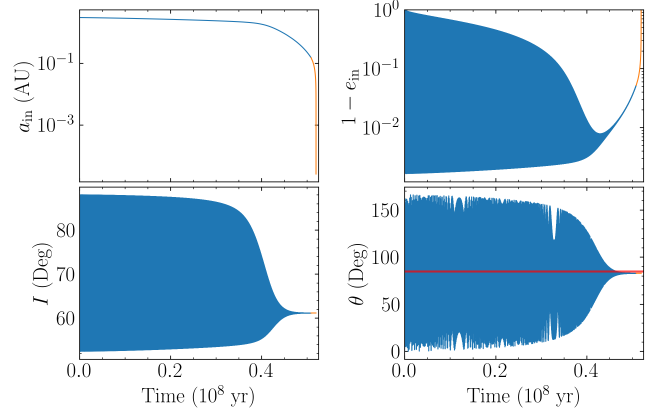


Figure 1. A binary’s semi-major axis (top left), eccentricity (top right), inclination (bottom left), and spin-orbit misalignment angle θ (bottom-left) as it coalesces via the tertiary-induced merger channel in the vicinity of a SMBH. As the eccentricity and inclination oscillate periodically due to the ZLK effect, the enhanced emission of GW induces the BBH to merge. Note that θ experiences significant oscillations but eventually converges to the prediction of Eq. (40) (horizontal red line). For computational efficiency, the late stages of inspiral are performed in the absence of the tertiary and without tracking the spin phase; this is denoted by the orange line in all four panels. Parameters used are: $a_{\text{in},0} = 3$ AU, $a_{\text{out}} = 8000$ AU = 0.04 pc, $e_{\text{out}} = 0.6$, $m_1 = 33M_{\odot}$, $m_2 = 17M_{\odot}$, and $I_0 = 88^{\circ}$.

Taken together, the orbital evolution of the system is given by

$$\frac{d\mathbf{L}_{\text{in}}}{dt} = \left. \frac{d\mathbf{L}_{\text{in}}}{dt} \right|_{\text{N}} + \left. \frac{d\mathbf{L}_{\text{in}}}{dt} \right|_{\text{GW}}, \quad (23)$$

$$\frac{d\mathbf{e}_{\text{in}}}{dt} = \left. \frac{d\mathbf{e}_{\text{in}}}{dt} \right|_{\text{N}} + \left. \frac{d\mathbf{e}_{\text{in}}}{dt} \right|_{\text{GR}} + \left. \frac{d\mathbf{e}_{\text{in}}}{dt} \right|_{\text{GW}}, \quad (24)$$

$$\frac{d\mathbf{L}_{\text{out}}}{dt} = \left. \frac{d\mathbf{L}_{\text{out}}}{dt} \right|_{\text{N}}, \quad (25)$$

$$\frac{d\mathbf{e}_{\text{out}}}{dt} = \left. \frac{d\mathbf{e}_{\text{out}}}{dt} \right|_{\text{N}}. \quad (26)$$

An example of this evolution is shown in Fig. 1, where the enhanced GW radiation due to eccentricities generated by the ZLK effect are able to drive the BBH to merge in $\lesssim 10^8$ yr despite it being too wide to merge in isolation (Eq. 3). For computational efficiency, the full spin-orbit evolution is replaced with a simplified evolution consisting of just GW emission at late times ($a_{\text{in}} \lesssim 0.1$ AU) when the binary evolution is fully decoupled from the effect of the SMBH; this is shown as the orange lines in all panels of Fig. 1. The evolution is truncated when $e_{\text{in}} < 10^{-3}$; note that the binary is still well wide of the LVK frequency band (GW frequency 10 Hz, or $a_{\text{in}} \sim 10^{-7}$ AU) but will merge shortly.

2.2. Spin Evolution: An Adiabatic Invariant

As the BBH gradually coalesces, the spins of the component black holes also evolve. At leading, 1-PN order, spin-spin coupling can be neglected (Racine 2008; Liu & Lai 2018), so the evolution of the two BHs can be treated independently. Thus, we will study the evolution of $\mathbf{S}_1 = S_1 \hat{\mathbf{s}}_1$ the spin of m_1 , though the evolution of \mathbf{S}_2 proceeds analogously. For brevity, we will drop the subscript. The de Sitter precession of $\hat{\mathbf{s}}$ about $\hat{\mathbf{J}}_{\text{in}}$ is given by (e.g. Barker & O'Connell 1975; Liu & Lai 2018)

$$\frac{d\hat{\mathbf{s}}}{dt} = \Omega_{\text{dS}} \hat{\mathbf{J}}_{\text{in}} \times \hat{\mathbf{s}}, \quad (27)$$

$$\Omega_{\text{dS}} = \frac{3Gn_{\text{in}}(m_2 + \mu_{\text{in}}/3)}{2c^2 a_{\text{in}} j_{\text{in}}^2}. \quad (28)$$

Recall that the observables χ_{eff} and χ_{p} (Eqs. 1, 2) depend on the misalignment angle $\theta = \cos^{-1}(\hat{\mathbf{s}} \cdot \hat{\mathbf{J}}_{\text{in}})$. The evolution of θ is shown in the bottom-right panel of Fig. 1 (see also Liu & Lai 2018; Su et al. 2021a). While θ appears to converge to its mean value by the end of the evolution, such a behavior is not an obvious consequence of the spin evolution given by Eq. (27): there is no dissipation!

Instead, the mechanism for this convergence is due to an unexpected adiabatic invariant (Liu & Lai 2017; Su et al. 2021a; see also Yu et al. 2020). Here, we present an abbreviated, qualitative description of the spin evolution; see Su et al. (2021a) for further details. For simplicity, we will assume that \mathbf{L}_{out} is approximately fixed and that $\epsilon_{\text{oct}}, \epsilon_{\text{SA}} \ll 1$, well satisfied for our fiducial parameters. Note that, as $\hat{\mathbf{s}}$ precesses about $\hat{\mathbf{J}}_{\text{in}}$ due to de Sitter precession, the orientation of $\hat{\mathbf{J}}_{\text{in}}$ itself also changes over the characteristic quadrupole-order ZLK timescale

$$\frac{1}{t_{\text{ZLK}}} = n_{\text{in}} \frac{m_3}{m_{12}} \left(\frac{a_{\text{in}}}{\tilde{a}_{\text{out}}} \right)^3, \quad (29)$$

$$\begin{aligned} &= \frac{1}{10^4 \text{ yr}} \left(\frac{m_3}{10^7 M_{\odot}} \right) \left(\frac{m_{12}}{70 M_{\odot}} \right)^{-1/2} \\ &\quad \times \left(\frac{a_{\text{in}}}{2 \text{ AU}} \right)^{3/2} \left(\frac{\tilde{a}_{\text{out}}}{6000 \text{ AU}} \right)^{3/2}. \end{aligned} \quad (30)$$

where $\tilde{a}_{\text{out}} \equiv a_{\text{out}} j_{\text{out}}$. Specifically $\hat{\mathbf{J}}_{\text{in}}$ both precesses and *nutates* (changing I) about $\hat{\mathbf{J}}_{\text{out}}$.

Depending on the value of $\Omega_{\text{dS}} t_{\text{ZLK}}$, there can be two regimes of evolution:

- First, if $\Omega_{\text{dS}} t_{\text{ZLK}} \ll 1$ (GR effects are weak), then de Sitter precession is too slow to drive precession of $\hat{\mathbf{s}}$ about the instantaneous orientation of the rapidly-varying $\hat{\mathbf{J}}_{\text{in}}$. As a result, $\hat{\mathbf{s}}$ instead precesses about some suitably time-averaged axis, which we discuss below.

- Second, if $\Omega_{\text{dS}} t_{\text{ZLK}} \gg 1$ (GR effects are strong), then de Sitter precession is sufficiently rapid that $\hat{\mathbf{s}}$ can efficiently follow the slow variations of $\hat{\mathbf{J}}_{\text{in}}$. As a result, θ remains approximately constant, as an action of the spin Hamiltonian (Landau & Lifshitz 1969).

In the first regime, the appropriate time averaging can be identified by treating the spin evolution as an iterative map over successive ZLK cycles.

$$\begin{aligned} \frac{\hat{\mathbf{s}}_{k+1} - \hat{\mathbf{s}}_k}{P_{\text{ZLK}}} &= \int_{t_0}^{t_0 + P_{\text{ZLK}}} \Omega_{\text{dS}} \hat{\mathbf{J}}_{\text{in}} \times \hat{\mathbf{s}} dt \\ &\approx \left[\int_{t_0}^{t_0 + P_{\text{ZLK}}} \Omega_{\text{dS}} \hat{\mathbf{J}}_{\text{in}} dt \right] \times \hat{\mathbf{s}}_k \\ &\equiv \langle \Omega_{\text{dS}} \hat{\mathbf{J}}_{\text{in}} \rangle \times \hat{\mathbf{s}}_k, \end{aligned} \quad (31)$$

where the angle brackets denote averaging over a ZLK cycle. Thus, over timescales $\gg P_{\text{ZLK}}$, the average spin evolution can be described by

$$\left\langle \frac{d\hat{\mathbf{s}}}{dt} \right\rangle = \langle \Omega_{\text{dS}} \hat{\mathbf{J}}_{\text{in}} \rangle \times \hat{\mathbf{s}}. \quad (32)$$

However, this expression is still difficult to analyze, since the orientation of $\langle \hat{\mathbf{J}}_{\text{in}} \rangle$ still varies on timescales $\sim P_{\text{ZLK}}$: Namely, while its nutation has been eliminated by the averaging, it will continue to precess about $\hat{\mathbf{J}}_{\text{out}}$ at a rate dominated by the quadrupolar-order ZLK evolution (e.g. Liu et al. 2015a; Su et al. 2021a):

$$\frac{d\langle \hat{\mathbf{J}}_{\text{in}} \rangle}{dt} \approx \langle \Omega_{\text{ZLK}} \rangle (\hat{\mathbf{J}}_{\text{out}} \times \langle \hat{\mathbf{J}}_{\text{in}} \rangle), \quad (33)$$

$$\Omega_{\text{ZLK}} \equiv \frac{3}{4t_{\text{ZLK}}} \frac{\cos I (5e_{\text{in}}^2 \cos^2 \omega_{\text{in}} - 4e_{\text{in}}^2 - 1)}{j_{\text{in}}}. \quad (34)$$

where ω_{in} is the argument of pericenter of the inner binary. To eliminate this precession, we perform a change of reference frame from Eq. (32) to the co-precessing frame, obtaining

$$\begin{aligned} \left\langle \frac{d\hat{\mathbf{s}}}{dt} \right\rangle_{\text{co-pre}} &= [\langle \Omega_{\text{dS}} \hat{\mathbf{J}}_{\text{in}} \rangle - \langle \Omega_{\text{ZLK}} \rangle \hat{\mathbf{J}}_{\text{out}}] \times \hat{\mathbf{s}} \\ &\equiv \mathbf{\Omega}_{\text{eff}} \times \hat{\mathbf{s}}. \end{aligned} \quad (35)$$

In this reference frame, $\mathbf{\Omega}_{\text{eff}}$ varies little over successive ZLK cycles, and only evolves gradually due to GW emission¹. Thus, as long as the GW-driven evolution of the

¹ Note that large ϵ_{oct} , large ϵ_{SA} , or spin-orbit resonances also result in substantial variation of $\mathbf{\Omega}_{\text{eff}}$ between successive ZLK cycles. These all result in non-conservation of θ_{eff} , which leads to unpredictable spin evolution (Liu & Lai 2018; Liu et al. 2019a; Su et al. 2021a).

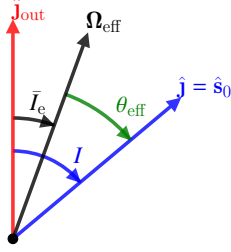


Figure 2. Notation of angles used to describe the adiabatic invariant in Section 2.2. Ω_{eff} is the effective spin precession axis, given by Eq. (35). Note that initially, $\hat{\mathbf{s}}_0 = \hat{\mathbf{j}}$, and so $\theta_{\text{eff}} = |\bar{I}_e - I_0|$, as shown.

system (Eq. 21) is much slower than P_{ZLK} , the angle

$$\theta_{\text{eff}} \equiv \cos^{-1}(\hat{\mathbf{s}} \cdot \hat{\Omega}_{\text{eff}}), \quad (36)$$

is an adiabatic invariant.

With this adiabatic invariant, it proves straightforward to understand the final spin-orbit misalignment angle θ . First, note that

$$\cos \theta_{\text{eff}} = \frac{\hat{\mathbf{s}} \cdot \langle \Omega_{\text{dS}} \hat{\mathbf{j}}_{\text{in}} \rangle - \hat{\mathbf{s}} \cdot \hat{\mathbf{j}}_{\text{out}} \langle \Omega_{\text{ZLK}} \rangle}{\Omega_{\text{eff}}}, \quad (37)$$

where $\langle \Omega_{\text{ZLK}} \rangle = \Delta \Omega_{\text{in}} / P_{\text{ZLK}}$, the average rate of change of Ω_{in} in an orbital period. At late times, when $\Omega_{\text{dS}} \gg \Omega_{\text{ZLK}}$, we see that $\theta_{\text{eff}} \approx \theta$. Thus, the final spin-orbit misalignment angle can be well-predicted by the initial value of θ_{eff} (denoted $\theta_{\text{eff},0}$) and its subsequent conservation.

To understand the scalings that govern $\theta_{\text{eff},0}$, we will specialize to the case where $\hat{\mathbf{s}}_0 \parallel \hat{\mathbf{j}}_{\text{in}}$ (a common assumption, e.g. Liu & Lai 2017, 2018; Liu et al. 2019a). For the wide binaries studied in the literature, and the “90° attractor” (Liu & Lai 2018; Su et al. 2021a), $\Omega_{\text{dS}} \ll \Omega_{\text{ZLK}}$ initially, and Eq. (37) immediately implies that $\cos \theta_{\text{eff},0} = \cos I_0$, which is nearly zero for nearly-perpendicular mutual inclinations of the inner and outer orbits necessary to drive wide binaries to extreme, merger-capable eccentricities.

In this paper, we will consider the regime where Ω_{dS} is not so much smaller than Ω_{ZLK} initially, and so we must be more precise. When also adopting initial spin-orbit alignment (well-justified in our mechanism, see Section 3), we have that $\hat{\mathbf{s}}_0$, $\langle \Omega_{\text{dS}} \hat{\mathbf{j}}_{\text{in}} \rangle$, and $\hat{\mathbf{j}}_{\text{out}}$ are all coplanar (in the co-precessing frame). Then, since the angle between $\hat{\mathbf{s}}_0$ and $\hat{\mathbf{j}}_{\text{out}}$ is just I_0 , it proves easiest to evaluate the angle between $\langle \Omega_{\text{dS}} \hat{\mathbf{j}}_{\text{in}} \rangle$ and $\hat{\mathbf{j}}_{\text{out}}$ (\bar{I}_e in the notation of Su et al. 2021a) in order to constrain $\theta_{\text{eff},0}$

(see Fig. 2). This is straightforward:

$$\sin \bar{I}_e = \frac{\langle \Omega_{\text{dS}} \hat{\mathbf{j}}_{\text{in},\perp} \rangle}{\langle \Omega_{\text{dS}} \hat{\mathbf{j}}_{\text{in},\parallel} \rangle - \langle \Omega_{\text{ZLK}} \rangle}, \quad (38)$$

$$\theta_{\text{eff},0} = |\bar{I}_e - I_0|. \quad (39)$$

Here, the \perp and \parallel subscripts denote the components of $\hat{\mathbf{j}}_{\text{in}}$ normal to and parallel to $\hat{\mathbf{j}}_{\text{out}}$. To obtain an even simpler expression at the cost of some accuracy, we can further approximate $\langle \Omega_{\text{dS}} \hat{\mathbf{j}}_{\text{in},\parallel} \rangle \ll \langle \Omega_{\text{dS}} \hat{\mathbf{j}}_{\text{in},\perp} \rangle \ll \Omega_{\text{ZLK}}$ (corresponding to large I_0 and weak spin-orbit coupling) and $I_0 \approx 90^\circ$ to obtain

$$\theta_{\text{eff},0} \simeq |\bar{\mathcal{A}}_0 - I_0|, \quad (40)$$

$$\begin{aligned} \bar{\mathcal{A}}_0 &\equiv \frac{|\langle \Omega_{\text{dS}} \hat{\mathbf{j}}_{\text{in}} \rangle|}{\langle \Omega_{\text{ZLK}} \rangle} \\ &= \frac{3Gm_{12}(m_2 + \mu_{\text{in}}/3)a_{\text{out}}^3 j_{\text{out}}^3}{2c^2 m_3 a_{\text{in},0}^4} \\ &\quad \times \tilde{\mathcal{A}}(a_{\text{in},0}, I_0, \dots), \end{aligned} \quad (41)$$

$$\cos \theta_{\text{eff},0} \simeq \cos I_0 - \bar{\mathcal{A}}_0. \quad (42)$$

where $\tilde{\mathcal{A}}$ is some dimensionless function that primarily captures the scaling of Ω_{dS} and Ω_{ZLK} with $e_{\text{in,max}}$. The accuracy of Eq. (40) is illustrated as the horizontal green line in the bottom-right panel of Fig. 1. We see that in the limit $\bar{\mathcal{A}}_0 \rightarrow 0$ and $I_0 \approx 90^\circ$ that we recover the 90° attractor result. However, for more compact binaries, \mathcal{A} is not so small, and a positive bias in the observed θ distribution arises, consistent with the LVK constraints (as discussed in Section 1).

We compare these analytical results to direct numerical integrations performed with a few values of $a_{\text{in},0} \in \{2, 3, 4, 5\}$ AU in Fig. 3. In the top panel, we show the merger times of the BBH systems that successfully merge within the duration of the numerical integration, 1 Gyr. In the middle panel, we show that the resulting misalignment angles can be well-described by Eq. (40). The central dip is because $\Omega_{\text{ZLK}} \rightarrow 0$ as $I \rightarrow 90^\circ$, and the effective precession axis is aligned with $\hat{\mathbf{j}}_{\text{in}}$ at all times (Su et al. 2021a). Other deviations from the analytical result likely arise from non-adiabaticity or resonances, both of which can be obtained from a more careful analysis than presented here (Su et al. 2021a). Finally, in the bottom panel, we show the spin-orbit misalignment angle distributions at each $a_{\text{in},0}$. The distributions broadly follow, but deviate noticeably, from the naive $a_{\text{in},0}^{-4}$ scaling predicted by Eq. (42). This is expected, as $\bar{\mathcal{A}}_0 \lesssim \cos I_0$ for much of our parameter space, violating the approximation used to derive Eq. (42).

It is important to note that the correlation between $a_{\text{in},0}$ and θ , a result of Eq. (40), relies on the assumption that $\hat{\mathbf{s}}_0 \parallel \hat{\mathbf{j}}_{\text{in},0}$, a limiting assumption that was

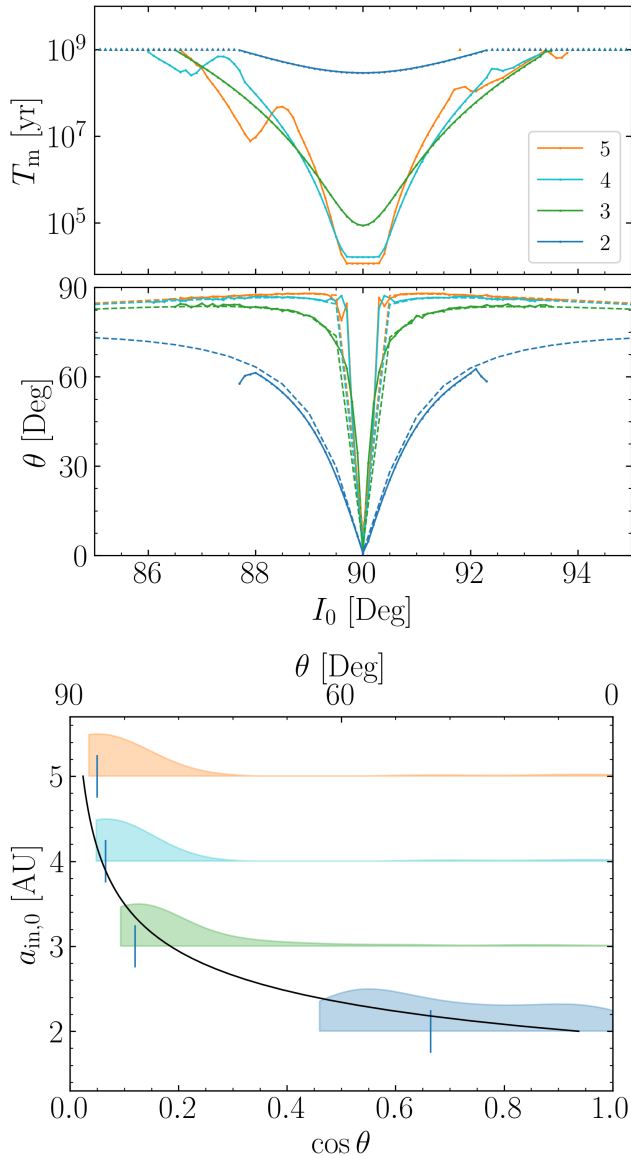


Figure 3. In these plots, we show how the final spin orientations of tertiary-induced BBH mergers change with their initial semi-major axis (we choose to vary $a_{in,0} \in \{2, 3, 4, 5\}$ AU) across a range of initial mutual inclinations I_0 between the inner and outer orbits. In the top panel, we show the merger times as a function of I_0 and $a_{in,0}$ (legend), where systems that evolve for longer than 1 Gyr are labeled with triangles (and likely become unbound by relaxation processes in the NSC). In the middle panel, we show the resulting misalignment angles for all merging systems. For each value of $a_{in,0}$, we also show the numerical evaluation of Eq. (40) in the correspondingly-colored dashed lines; good agreement is seen. Finally, in the bottom panel, we show the histograms of misalignment angles θ obtained at each value of $a_{in,0}$, and we have overlaid an arbitrary $a_{in,0}^{-4}$ line (predicted by Eq. 42) to guide the eye. All parameters other than those labelled are the same as in Fig. 1.

also pointed out in Yu et al. (2020). For dynamically-assembled BBHs, such an assumption cannot be made, as the component BH spins are randomly oriented upon capture. For BBHs born from wide stellar binaries, there are two issues with this initial condition: the spins of the stars need not be aligned with the orbits of their wide binary companions at birth, and the birth of the BHs will significantly modify the orbit due to supernova (SN) kicks (e.g. Rodriguez et al. 2016). On the other hand, for more compact BBHs, this is a sensible initial condition because the Keplerian orbital velocity of the binary becomes larger than the natal kick velocity, and because the stellar spins are likely well-aligned with the orbit (whether because the stars are co-natal or due to alignment processes such as mass transfer).

On its own, a correlation between $a_{in,0}$ and θ is not so useful, as $a_{in,0}$ is a property of the BBH at its formation rather than when it is observed by LVK. However, if $a_{in,0}$ is correlated with other properties of the BBH, then the mechanism we’ve discussed can introduce additional structures to the observed parameters of BBH systems. In the next section, we show that a preceding phase of binary stellar evolution can introduce such correlations.

3. STELLAR BINARY EVOLUTION

As the origin of the BBHs considered in the previous section, we consider that they may be the final evolutionary stage of stellar binaries orbiting a SMBH. Observationally, stellar binaries have been found within ~ 0.1 pc of Sgr A* (Martins et al. 2006; Pfuhl et al. 2014; Peißker et al. 2024), consistent with the binary fraction of young star clusters (Alexander 2017). On the other hand, more recent studies identify a deficit of massive stellar binaries within the central 0.02 pc of Sgr A* (Chu et al. 2023). Nevertheless, as the formation of nuclear star clusters (NSCs) is not well understood (see e.g. Neumayer et al. 2020, for a recent review), it appears plausible that massive stellar binaries can be formed as close in as ~ 0.04 pc to a central SMBH (corresponding to our fiducial parameters) on eccentric orbits (Ali et al. 2020). Additionally, due to the low efficiency of dynamical binary formation so near an SMBH, where the velocity dispersion is very large (e.g. Hut 1985; Quinlan & Shapiro 1989), it is likely that any BBHs so close to their central SMBHs either formed as a primordial stellar binary or formed via gas-assisted capture in an active galactic nucleus (AGN) disk (e.g. Bartos et al. 2017). In this section, we focus on the former possibility and defer discussion the latter to many other excellent works (see Section 6).

In this section, we consider an initial stellar binary with total mass $m_{12,*} = 100M_\odot$ at semi-major axis

$a_{\text{in},\star} = 2 \text{ AU}$, and with the same outer orbital parameters used above in Section 2.2. We will study the resulting spin misalignment of the merging BBH as a function of the BBH mass ratio q_{BH} by varying the mass ratio of the initial stellar binary q_{\star} .

3.1. Short Range Force Suppression of ZLK

First, we address one key ingredient for this mechanism. In order for the $a_{\text{in},\star} \sim \text{AU}$ stellar binary to form a $a_{\text{in}} \sim \text{AU}$ BBH that subsequently merges, it must not experience ZLK-driven coalescence, but the BBH must reach sufficiently large eccentricities via ZLK to be driven towards merger. One way that this can be accomplished is by reorienting the binary between its stellar and BH phases, either via collective effects such as resonant relaxation (Rauch & Tremaine 1996) or via natal kicks (e.g. Vigna-Gómez et al. 2024). We consider a second possibility, that the additional short range forces (SRFs) present in stellar binaries are able to suppress ZLK (e.g. Kiseleva et al. 1998; Eggleton & Kiseleva-Eggleton 2001; Wu & Murray 2003; Liu et al. 2015a) while those in the subsequent BBH cannot.

In a stellar binary, Eq. (5) for the evolution of \mathbf{e}_{in} has two extra terms due to apsidal precession driven by the rotational and tidal bulges of the two stars (e.g. Liu et al. 2015a). The contributions from the primary are given by (Kiseleva et al. 1998; Liu et al. 2015a)

$$\left. \frac{d\mathbf{e}_{\text{in}}}{dt} \right|_{\text{Rot},1} = \frac{k_{q,1} \Omega_{1s}^2 R_1^5}{G a_{\text{in}}^2 m_2 j_{\text{in}}^4} n_{\text{in}} \hat{\mathbf{j}}_{\text{in}} \times \mathbf{e}_{\text{in}}, \quad (43)$$

$$\left. \frac{d\mathbf{e}_{\text{in}}}{dt} \right|_{\text{Tide},1} = \frac{15 k_{2,1} R_1^5 m_1}{a_{\text{in}}^5 m_2 j_{\text{in}}^{10}} f(e_{\text{in}}) n_{\text{in}} \hat{\mathbf{j}}_{\text{in}} \times \mathbf{e}_{\text{in}}, \quad (44)$$

$$f(e_{\text{in}}) = \left(1 + \frac{3e_{\text{in}}^2}{2} + \frac{e_{\text{in}}^4}{8} \right).$$

and the corresponding contributions from the secondary are obtained by interchanging the indices $1 \leftrightarrow 2$. Here, $k_{q,1} = k_{2,1}$ is the apsidal motion constant, while $k_{2,1}$ is the tidal Love number, Ω_{1s} is the spin frequency of the primary, and R_1 is its radius.

Given the combination of the three SRFs (GR, tides, and rotation), the maximum eccentricity $e_{\text{in,max}}$ that can be attained via the ZLK effect (when $I = 90^\circ$) is given by (Liu et al. 2015b)

$$\begin{aligned} & \frac{\epsilon_{\text{tide},1}}{15} \left(\frac{1 + 3e_{\text{in,max}}^2 + \frac{3e_{\text{in,max}}^4}{8}}{j_{\text{in,min}}^9} - 1 \right) \\ & + \frac{\epsilon_{\text{rot},1}}{3} \left(\frac{1}{j_{\text{in,min}}^3} - 1 \right) \\ & + \epsilon_{\text{GR}} \left(\frac{1}{j_{\text{in,min}}} - 1 \right) = \frac{9}{8} e_{\text{in,max}}^2, \end{aligned} \quad (45)$$

where the three dimensionless parameters quantifying the relative strengths of the general relativistic, tidal, and rotational apsidal precession effects are given by

$$\epsilon_{\text{GR}} = \frac{3Gm_{12}^2 \tilde{a}_{\text{out}}^3}{a_{\text{in}}^4 c^2 m_3}, \quad (46)$$

$$\epsilon_{\text{tide},1} = \frac{15m_1 m_{12} \tilde{a}_{\text{out}}^3 k_{2,1} R_1^5}{a_{\text{in}}^8 m_2 m_3}, \quad (47)$$

$$\epsilon_{\text{rot},1} = \frac{m_{12} \tilde{a}_{\text{out}}^3 k_{2,1} R_1^5}{2G a_{\text{in}}^5 m_2 m_3} \Omega_{1s}^2, \quad (48)$$

and $j_{\text{in,min}} \equiv \sqrt{1 - e_{\text{in,max}}^2}$. Eq. (45) can be straightforwardly generalized to include the contributions from the secondary (i.e. $\epsilon_{\text{tide},2}$ and $\epsilon_{\text{rot},2}$). However, while the combined precessional effects will further suppress eccentricity excitation, the disparate mass ratios in our considered systems imply that the SRFs due to either the primary or the secondary (after the primary has evolved into a BH) will dominate the apsidal precession of the binary. As such, it is sufficient to consider only one set of SRFs at a time.

In a stellar binary, the dominant SRF is apsidal precession driven by either the rotational or tidal bulges of the stars. For our fiducial parameters, the stellar tidal synchronization timescale due to the equilibrium tide is (Alexander 1973; Hut 1981; Lai 2012):

$$\begin{aligned} \frac{1}{t_s} &= \frac{1}{4k} \frac{3k_2}{Q} \left(\frac{m_2}{m_1} \right) \left(\frac{R_1}{a_{\text{in}}} \right)^3 n_{\text{in}} \\ &= \frac{1}{1 \text{ Gyr}} \left(\frac{2k_2/Q}{10^{-6}} \right) \left(\frac{m_2}{m_1} \right) \left(\frac{R_1}{10R_\odot} \right)^3 \left(\frac{a_{\text{in}}}{2 \text{ AU}} \right)^{-9/2}. \end{aligned} \quad (49)$$

As such, the stars remain rapidly rotating throughout their MS lifetimes ($\lesssim \text{Myr}$), and the rotational bulge provides the dominant source of apsidal precession to truncate the ZLK cycles. Note that, when other SRFs are negligible, Eq. (45) reduces to

$$\frac{8\epsilon_{\text{rot}}}{27} = \frac{j_{1,\text{min}}^3 (1 + j_{1,\text{min}})}{1 + j_{1,\text{min}} + j_{1,\text{min}}^2}. \quad (50)$$

Thus, we conclude that $\epsilon_{\text{rot}} \geq 9/4$ suppresses ZLK oscillations entirely ($j_{1,\text{min}} = 1$; see Fig. 6 of Liu et al. 2015b). For our fiducial parameters,

$$\begin{aligned} \epsilon_{\text{rot},1} &= 2.3 \frac{m_{1,\star}}{m_{2,\star}} \left(\frac{k_{q,1}}{0.02} \right) \left(\frac{m_{12,\star}}{100M_\odot} \right) \left(\frac{\tilde{a}_{\text{out}}}{6400 \text{ AU}} \right)^3 \\ &\times \left(\frac{R_1}{10R_\odot} \right)^2 \left(\frac{a_{\text{in},\star}}{2\text{AU}} \right)^{-5} \left(\frac{m_3}{10^7 M_\odot} \right)^{-1} \\ &\times \left(\frac{\Omega_{s,1}/\Omega_{\text{dyn},1}}{0.8} \right)^2, \end{aligned} \quad (51)$$

where $\Omega_{\text{dyn},1} \equiv \sqrt{Gm_{1,*}/R_1^3}$ is the dynamical frequency of the primary and is also its maximal spin frequency. We have taken values for the stellar structure from numerical simulations using Modules for Experiments in Stellar Astrophysics (MESA Paxton et al. 2011, 2013, 2015, 2018, 2019; Jermyn et al. 2023) representative of a $60M_\odot$ star for solar and sub-solar metallicities along its main sequence. As such, we conclude that the rotational bulge of the primary is able to suppress ZLK oscillations for our fiducial parameters. As will become clear below, this suppression is active until both stars collapse to BHs.

To complete the picture, once the stellar binary forms a BBH, the only SRF is the apsidal precession due to first-order post-Newtonian effects. In the absence of other SRFs, Eq. (45) reduces to

$$\frac{8\epsilon_{\text{GR}}}{9} = j_{1,\text{min}} (1 + j_{1,\text{min}}). \quad (52)$$

Thus, we find that $\epsilon_{\text{GR}} \gtrsim 9/4$ suppresses ZLK entirely (see Fig. 6 of Liu et al. 2015b). For fiducial parameters, ϵ_{GR} evaluates to

$$\begin{aligned} \epsilon_{\text{GR}} = 0.12 & \left(\frac{m_{12}}{50M_\odot} \right)^2 \left(\frac{\tilde{a}_{\text{out}}}{6400 \text{ AU}} \right)^3 \\ & \times \left(\frac{a_{\text{in}}}{2\text{AU}} \right)^{-4} \left(\frac{m_3}{10^7 M_\odot} \right)^{-1}. \end{aligned} \quad (53)$$

Note that $m_{12} < m_{12,*}$ due to mass loss during binary stellar evolution. Thus, we find that eccentricity excitation via the ZLK effect can be achieved during the BH phase even as it is suppressed during the stellar phase.

3.2. Binary Stellar Evolution: Double Stable Mass Transfer

Given that the stellar binary, consisting of two stars with zero-age main sequence (ZAMS) masses $m_{1,*}$ and $m_{2,*}$ does not experience ZLK oscillations, it will evolve undergoing standard isolated binary evolution. In traditional prescriptions, such evolution results in one phase of stable mass transfer followed by a second phase of unstable mass transfer (a common envelope phase), leading to a very compact binary that may even successfully merge in isolation (e.g. Hurley et al. 2002; Belczynski et al. 2016). However, more recent studies suggest that, except for very extreme mass ratios ($q_* \equiv m_{2,*}/m_{1,*} \lesssim 0.2$), many stellar binaries that form compact object binaries may instead undergo two phases of stable mass transfer (MT) (e.g. Gallegos-Garcia et al. 2021; van Son et al. 2022). As the detailed physics of these two phases of MT are still filled with uncertainties, we can gain some qualitative understanding of the parameter space that

can result by implementing simple analytical prescriptions. In general, the final outcome of MT will depend on the stellar properties, and will introduce correlations between the initial a_{in} of the BBH and its various other physical properties. We describe the double MT phase using the formalism of Soberman et al. (1997) (S97) and use similar parameters as modern works (e.g. van Son et al. 2022; Riley et al. 2022).

In the S97 formalism, as a star $m_{1,*}$ initiates MT, the mass lost from the star follows one of three modes. The first is called Jeans's mode or the fast mode (Soberman et al. 1997), in which a spherically symmetric outflow directly removes matter from $m_{1,*}$, carrying away the specific angular momentum of the donor star. The second is called isotropic re-emission, in which matter is first transferred to the vicinity of the accretor before being rapidly, isotropically ejected; matter lost in this fashion carries away the specific angular momentum of the accretor instead. The third is accretion, in which the matter lost from $m_{1,*}$ is deposited onto $m_{2,*}$, conserving the total angular momentum of the system. A given MT phase can be parameterized by the fractions α , β , and ϵ , which denote the fraction of matter lost from the primary via either the fast mode, isotropic re-emission, or accretion respectively; note that $\alpha + \beta + \epsilon = 1$ (we do not consider mass loss through L2, which becomes important for rapid mass loss, Soberman et al. 1997; Lu et al. 2023). Then, the effect on the orbit is most easily expressed as the change in the orbit's angular momentum (Soberman et al. 1997)²:

$$\frac{L_f}{L_0} = \begin{cases} \left(\frac{q_f}{q_0} \right)^\alpha \left(\frac{1+q_f}{1+q_0} \right)^{-1} \left(\frac{1+\epsilon q_f}{1+\epsilon q_0} \right)^C & \epsilon > 0, \\ \left(\frac{q_f}{q_0} \right)^\alpha \left(\frac{1+q_f}{1+q_0} \right)^{-1} e^{\beta(q_f - q_0)} & \epsilon = 0, \end{cases}, \quad (54)$$

where L_0 and L_f are the initial and final angular momentum of the binary, q_0 and q_f are its initial and final mass ratio, and

$$C = \frac{\alpha\epsilon}{1-\epsilon} + \frac{\beta}{\epsilon(1-\epsilon)}. \quad (55)$$

Note that when $\alpha = \beta = 0$ and $C = \epsilon = 1$, we recover the standard result $L_f = L_0$ of fully conservative MT.

In this work, we will assume that, between the zero-age main sequence and the end of the mass transfer phase, the primary loses the entirety of its radiative envelope, and we denote f_{core} to be the core mass fraction

² We have set the fast mode angular momentum transfer enhancement factor in Soberman et al. (1997) $A = 1$, as in the wide binaries we consider, the spin angular momentum of the stars is negligible compared to that of the orbit.

of the primary (see e.g. [van Son et al. 2022](#)). For the high-mass stars we consider, $f_{\text{core}} \simeq 0.5$ (broadly consistent with the MIST stellar evolution tracks, [Dotter 2016](#); [Choi et al. 2016](#)), and as a first approximation we take this to be a constant; we will explore a mass-dependent f_{core} shortly. Then, the evolution from a ZAMS binary to a BBH is modeled in four separate stages:

- During the first phase, the primary ejects some fraction η_{wind} of its envelope mass, $(1 - f_{\text{core}})m_{1,*}$, due to stellar winds. The exact value of η_{wind} is currently not well-known for massive stars, but it is likely subdominant to binary-driven mass loss, implying that $\eta_{\text{wind}} \lesssim 0.5$. We take $\eta_{\text{wind}} = 0.2$ as a fiducial value.

Among this wind-ejected matter, we approximate that half will be unbound from the binary, and the other half will be accreted by the secondary (as seen in high-mass x-ray binaries, e.g. [Forasini et al. 2024](#)). Thus, we take $(\alpha_1, \beta_1, \epsilon_1) = (0.5, 0, 0.5)$ as fiducial values for this wind-driven mass loss phase.

- During the second phase, the primary ejects the remainder of its envelope (consisting of mass $(1 - \eta_{\text{wind}})(1 - f_{\text{core}})m_{1,*}$) on a thermal timescale. As such, the fast mode of mass loss is sufficiently weak to be neglected (e.g. [van Son et al. 2022](#)). Of the remaining mass, all of which reaches the vicinity of the secondary, some fails to be accreted and experiences isotropic re-emission.

For simplicity, let us define $\tilde{\beta}_2 \equiv \beta_2/(1 - \eta_{\text{wind}})$, and similarly for $\tilde{\epsilon}_2$. As such, the three quantities satisfying

$$\eta_{\text{wind}} + \tilde{\beta}_2 + \tilde{\epsilon}_2 = 1, \quad (56)$$

denote the mass fractions of the primary’s ejected envelope lost via stellar winds, isotropic-reemission during stable MT, and accretion during stable MT respectively. To account for this, we take fiducial values $(\tilde{\beta}_2, \tilde{\epsilon}_2) = (0.4, 0.4)$ for this mass transfer phase. This is implemented by evaluating Eq. (54) using $(\alpha, \beta, \epsilon) = (0, 1/2, 1/2)$.

After this phase, we model that the remaining mass of the primary, $f_{\text{core}}m_{1,*}$ experiences direct collapse to a BH with no natal kick (e.g. [Giacobbo & Mapelli 2020](#); [De et al. 2024](#)). The secondary has attained a new mass $m_{2,*} = m_{2,*\text{ZAMS}} + \tilde{\epsilon}_2(1 - f_{\text{core}})m_{1,*}$. Its new core mass is then $f_{\text{core}}m_{2,*}$, i.e. the convective-radiative boundary of the accretor adjusts to its new mass (and possibly “rejuvenating” the core, e.g. [Hellings 1983](#); [Renzo & Götzberg 2021](#), but see also [Braun & Langer 1995](#)).

- During the third phase, the secondary also experiences wind-driven mass loss. It also loses η_{wind} of its envelope, with $(\alpha_3, \beta_3, \epsilon_3) = (0.5, 0, 0.5)$.
- During the fourth phase, the secondary initiates a second phase of stable MT. Again, the fast mode is too slow to contribute to mass loss. However, additionally, the primary (which is now a BH) likely does not accrete efficiently, i.e. not much more rapidly than the strongly constraining Eddington limit ([van Son et al. 2022](#)); note that even sustained accretion at $\sim 10^2 L_{\text{edd}}$, as suggested by recent 3D radiation hydrodynamics simulations ([Toyouchi et al. 2024](#)), only leads to modest accretion during a stable MT episode. Due to the low accretion efficiency, almost all of the mass transferred from the secondary experiences isotropic re-emission. As such, we take $\tilde{\beta}_4 = 1$ and $\tilde{\epsilon}_4 = 0$ as fiducial values.

In summary, the four phases of the mass transfer procedure depend on a total of five free parameters: η_{wind} , $\tilde{\epsilon}_2$, $\tilde{\epsilon}_4$, and the two f_{core} values for the stars (recall that $\tilde{\beta}_2 = 1 - \eta_{\text{wind}} - \tilde{\epsilon}_2$ and similarly for $\tilde{\beta}_4$). By fixing $\tilde{\epsilon}_4 = 0$ and enforcing a shared f_{core} prescription for the two stars (either constant or mass-dependent), the number of free parameters is reduced to just three.

By applying this four-phase prescription for mass transfer, we obtain a relation between the stellar binary’s semi-major axis $a_{\text{in},*}$ and that of the BBH a_{in} (for consistency with the notation in Section 2, we omit the BH subscripts for quantities describing the BBH) as well as between the stellar binary’s mass ratio $q_{\text{in},*}$ and that of the BBH q_{in} . In Fig. 4, we show the binary evolution resulting from the four-phase MT prescription detailed above. First, we note in the top panel that mass ratio inversions are seen for near-equal-mass binaries (red line). Since the spins of the first and second-formed BHs are sometimes expected to differ (e.g. [Olejak et al. 2024](#)), we will keep track of mass ratio inversions. Note that the MT prescription we’ve proposed is scale-free and only yields predictions for the semi-major axis ratios rather than their specific values. Of course, physical models of MT yield dramatically different results depending on binary orbital separation, which would be modelled in our formalism as dependencies of $\tilde{\epsilon}_2$ and other parameters on $a_{\text{in},*}$.

There are two features about the evolution above that are essential to our subsequent discussion. First, note that $a_{\text{in}} \simeq a_{\text{in},*}$, i.e. the binary does not shrink appreciably during its evolution to a BBH, and ZLK oscillations are able to overcome. Second, the last panel of Fig. 4 shows that a_{in} and q_{in} are positively correlated. Then,

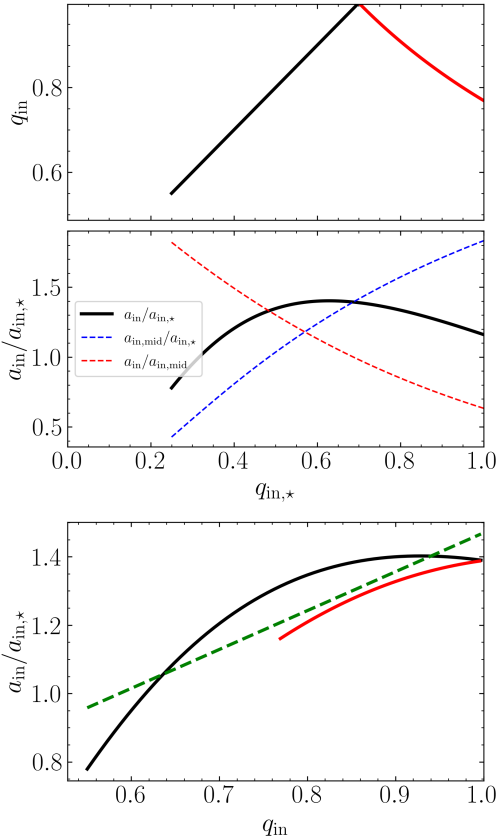


Figure 4. In the first panel, we show the final mass ratio q_f obtained after the four-step mass transfer prescription discussed in Section 3.2. The red line denotes systems that experience mass ratio inversion, where the more massive BH is formed from the initially less massive star, and the black line denotes systems that do not experience this inversion. In the middle panel, we illustrate the three pairwise ratios of the binary’s initial semi-major axis a_0 , its intermediate value (after the formation of the first BH, i.e. at the end of the second phase) a_i , and its final value (after the formation of both BHs) a_f . In the bottom panel, we show the resulting correlation between a_f and q_f , where the black and red lines have the same meaning as in the top panel. A positive correlation is seen, as depicted by the linear fit shown as the green dashed line. The parameters used here are $f_{\text{core}} = 0.5$, $\eta_{\text{wind}} = 0.2$, $\tilde{\epsilon}_2 = 0.4$, and $\tilde{\beta}_2 = 0.4$.

application of Eq. (40) suggests that the final spin-orbit misalignment will be *negatively* correlated with q_{in} ; this will be shown in Section 4.

To understand the robustness of these two features as a function of the three free parameters of the system, we study the dependence of the mean slope $da_{\text{in}}/dq_{\text{in}}$ (defined as the best fit line as shown in Fig. 4) and the mean semi-major axis change $\langle a_{\text{in}}/a_{\text{in},*} \rangle$ on the free parameters of the MT prescription. In Fig. 5, we show the dependence of these two quantities on η_{wind} , $\tilde{\epsilon}_2$ for three different f_{core} prescriptions: $f_{\text{core}} = 0.5$, $f_{\text{core}} =$

0.7, and a mass-dependent fraction

$$f_{\text{core}} = 0.4 + (m_{\star}/320M_{\odot}). \quad (57)$$

This simple prescription is in coarse agreement with asteroseismic and spectroscopic observations for lower masses (Tkachenko et al. 2020; Johnston 2021; Pedersen et al. 2021) and with the MIST evolutionary tracks at higher masses (Dotter 2016; Choi et al. 2016). Broadly, it can be seen that a positive correlation between a_{in} and q_{in} , as well as a gentle orbital softening, are robust features of our MT model.

As a final note, we comment on the intuitive reason for the observed correlation between a_{in} and q_{in} during our double MT prescription. First, conservative mass transfer generally drives small-mass-ratio systems closer to equal mass ratios. This effect is preferentially stronger for more unequal initial mass ratios. Since conservative mass transfer conserves $L_{\text{in}} \propto q_{\text{in},*} \sqrt{a_{\text{in},*}} / (1 + q_{\text{in},*})$, it can be seen that a larger increase in $q_{\text{in},*}$ corresponds to a larger decrease of $a_{\text{in},*}$. Accordingly, we find that BBHs formed with small q_{in} should also have small a_{in} . Second, isotropic re-emission leads to a similar correlation: since the ejected matter leaves with the specific angular momentum of the accretor, a smaller mass ratio ejects more angular momentum and results in more binary hardening. Finally, fast mode mass loss has a smaller effect on the orbital separation (since it is typically ejected from the more massive donor, and as such it carries away little angular momentum) but broadly leads to binary widening. Thus, the combination of all three mass loss mechanisms results in a combination of mass-ratio-dependent binary hardening and general wind-driven binary softening.

4. SIGNATURES IN BLACK HOLE MERGER PROPERTIES: ANTI-CORRELATION BETWEEN MASS RATIO AND SPIN-ORBIT MISALIGNMENT ANGLE

As shown in the previous section, a population of stellar binaries with fixed semi-major axis $a_{\text{in},*}$ and varying mass ratios $q_{\text{in},*}$ will yield a population of BBHs with positively correlated a_{in} and q_{in} . This will result in an anti-correlation between spin-orbit misalignment θ and q_{in} following the results of Section 2.2, namely Eq. (40). In this section, we use numerical integrations to explore the strength of this correlation and substantiate the analytical arguments made above.

For clarity, we consider a population of nearly-circular ($e_{\text{in}} = 10^{-3}$) stellar binaries with fixed total mass $m_{12,*} = 100M_{\odot}$, fixed semi-major axis $a_{\text{in},*}$, and with $q_{\text{in},*} \in [0.25, 1]$ (a standard MT stability threshold, e.g. Schneider et al. 2015; Temmink, K. D. et al. 2023). Us-

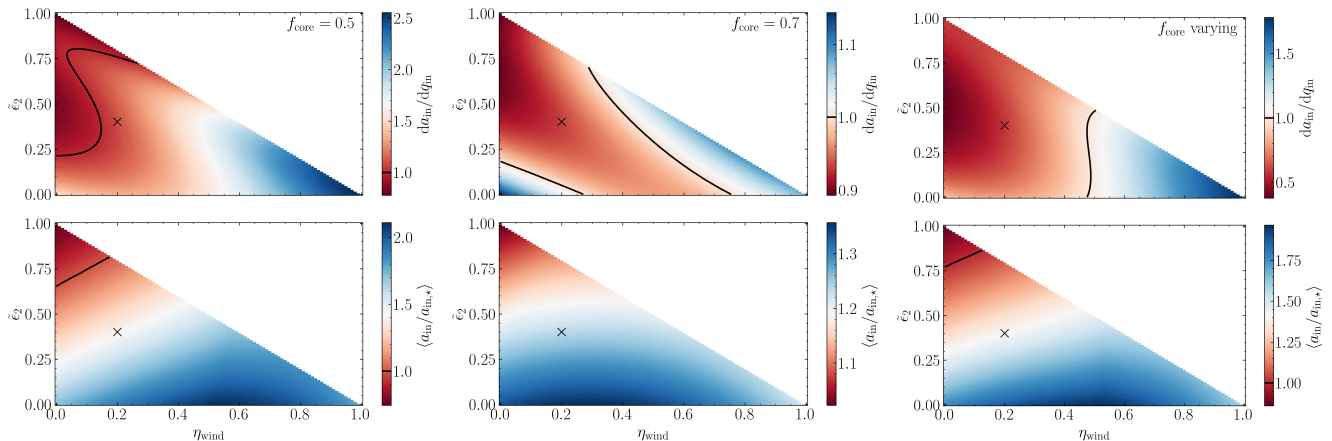


Figure 5. The left column of plots shows the values of the mean correlation $da_{\text{in}}/dq_{\text{in}}$ and the mean semi-major axis change $\langle a_{\text{in}}/a_{\text{in},*} \rangle$ as a function of η_{wind} and $\tilde{\epsilon}_2$, two of the three free parameters of the MT prescription laid out in Section 3.2; the third, f_{core} , is fixed at 0.5. The upper-right triangle in both plots is forbidden due to the requirement that $\eta_{\text{wind}} + \tilde{\epsilon}_2 + \tilde{\beta}_2 = 1$ (Eq. 56) and that $\tilde{\beta}_2 \geq 0$. The middle column of plots shows the same but for $f_{\text{core}} = 0.5$. The final column of plots shows the same but for a mass-dependent f_{core} (Eq. 57). In all panels, a value of 1 is shown as a black contour when within the scale of the color plot.

ing the results of the previous section, these stellar binaries evolve into BBHs via the MT prescription of Section 3.2 with semi-major axes a_{in} and mass ratios q_{in} . Then, for the orbital dynamics phase of evolution, these BBHs are assumed to have a random initial inclination with respect to the plane of their orbit around a central SMBH (though for computational efficiency we restrict I to values within the window of inclinations that can drive successful mergers as shown in the upper panels of Fig. 3). The remaining orbital elements are held fixed for simplicity: $\omega_{\text{in}} = 0$, $\omega_{\text{out}} = 0.7$, and $\Omega_{\text{in}} = \Omega_{\text{out}} - \pi = 0$. Finally, the initial spins of the BHs are aligned with the inner orbit normal, due to the multiple phases of MT. The inner and outer orbits and the spins of the BHs are then evolved following the equations of motion as described in Section 2 for 1 Gyr, which is significantly longer than the expected unbinding time for such binaries in typical NSC models (see Section 5). For systems that successfully merge, we record their merger time and final spin-orbit misalignment angle.

Note that we must account for the possibility that the rotational SRF (Eq. 51) may be too weak to suppress ZLK excitation after the formation of the first BH. To do so, we evaluate Eq. (51) at the end of the second MT phase (i.e. using $a_{\text{in,mid}}$ from Fig. 4) but, for simplicity, we hold the stellar parameters R_* and k_q constant at their fiducial values (which avoids having to introduce detailed stellar modeling, beyond the scope of this paper), and we set $\Omega_s/\Omega_{\text{dyn}} = 1$ for the secondary (which is spun up to near critical rotation by the MT from the primary). We then keep track of systems that pass through a state with $\epsilon_{\text{rot}} < 9/4$. While our crude approximations are unable to definitively conclude that such systems ex-

perience strong ZLK oscillations between the formation of the first and second BH, it suffices as a first estimate of susceptibility.

The properties of the systems that successfully merge are shown in Fig. 6, where blue points denote systems that may experience ZLK oscillations between the formation of the two compact objects based on the discussion immediately above. Such objects tend to have larger initial mass ratios, leading to more orbital expansion during the formation of the first BH (Fig. 4). A clear anti-correlation between q_{in} and θ can be seen both in the black points alone and in the entire population. The inferred fraction of systems (among all misalignment angles I between the inner and outer orbits, uniformly weighted in $\cos I$) that successfully merge within 1 Gyr is $\approx 6\%$, falling to $\approx 4\%$ when restricting to systems merging within 10 Myr; approximately 2/3 of these systems are susceptible to ZLK between the formation of the first and second BHs.

5. FEASIBILITY IN ASTROPHYSICAL SETTINGS

Above, we have shown that binary stars within the central regions of their SMBH may form merging BBHs with correlations in their spin-orbit misalignment thanks to their other physical properties due to two phases of stable MT. In this section, we assess the feasibility of the proposed mechanism in typical NSCs.

We first evaluate the dynamical lifetime of the binaries we consider. In order to do so, we adopt an NSC stellar density profile in line with recent studies (e.g. Rose et al. 2020; Jurado et al. 2024). While the standard theoretical result, the Bahcall-Wolf profile (Bahcall & Wolf 1976; Binney & Tremaine 2008) gives that

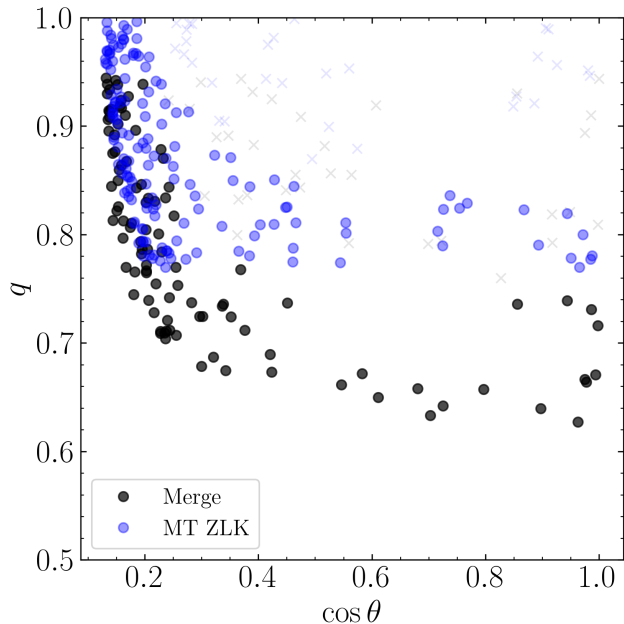


Figure 6. The properties of successfully merging BBH systems after the combined double mass transfer and orbital evolution summarized in Section 4, corresponding to the MT prescription shown in the left panels of Fig. 4. Black and red points denote systems that successfully merge, where red points correspond to a mass ratio inversion. Blue points denote systems that may be susceptible to ZLK during the double MT phase, during the interval between the formation of the first and second BHs (see Section 4). Circles denote systems merging within 10 Myr, while crosses denote systems merging between 10 Myr and 1 Gyr, the maximum length of the orbital integration.

$n(a_{\text{out}}) \propto a_{\text{out}}^{-\alpha}$ with $\alpha = 7/4$, observations of the Milky Way galactic center suggest a shallower profile, $\alpha \sim 1.1-1.4$ (Gallego-Cano et al. 2018), so we instead adopt a value of $\alpha = 1.5$. Then, when accounting for the standard M - σ relation (Tremaine et al. 2002), we obtain the following stellar density profile

$$\rho(a_{\text{out}}) = \frac{3 - \alpha}{2\pi} \frac{m_p}{a_{\text{out}}^3} \left(\frac{G\sqrt{m_p M_0}}{\sigma_0^2 a_{\text{out}}} \right)^{\alpha-3}, \quad (58)$$

where $M_0 = 10^8 M_\odot$ and $\sigma_0 = 200$ km/s are the standard normalization, and m_p is the typical mass of stars in the NSC. In such a cluster, the velocity dispersion that our fiducial binary experiences is

$$\begin{aligned} \sigma(a_{\text{out}}) &= \sqrt{\frac{Gm_3}{a_{\text{out}}(1 + \alpha)}} \\ &= 700 \text{ km/s} \left(\frac{m_3}{10^7 M_\odot} \right)^{1/2} \left(\frac{a_{\text{out}}}{0.04 \text{ pc}} \right)^{-1/2}. \end{aligned} \quad (59)$$

From this, we can calculate the characteristic binary dissociation/evaporation timescale

$$t_{\text{evap}} = \frac{\sqrt{3}\sigma(a_{\text{out}})}{32\sqrt{\pi}G\rho(r)a_{\text{in}}\ln(\Lambda)} \frac{m_{12}}{m_p}. \quad (60)$$

Here, $\ln \Lambda = 5$ is the Coulomb algorithm, we use $m_p = m_{12}/2$ is the mass of flyby stars. For our fiducial parameters, this yields $t_{\text{evap}} \simeq 10$ Myr.

Another constraint on the system properties arises from enforcing dynamical stability of the triple. For dynamical stability, we adopt the often used (Mardling & Aarseth 2001) condition for dynamical stability:

$$\frac{a_{\text{out}}}{a_{\text{in}}} \gtrsim 2.8 \left(1 + \frac{m_3}{m_{12}} \right)^{2/5} \frac{(1 + e_{\text{out}})^{2/5}}{(1 - e_{\text{out}})^{6/5}} \left(1 - 0.3 \frac{I_{\text{tot,d}}}{180^\circ} \right). \quad (61)$$

For our fiducial parameters, the right-hand side of this expression is ~ 1500 (taking $I_{\text{tot,d}} \simeq 90^\circ$, and adopting $m_{12} = 50 M_\odot$, the final BH value), while the left-hand side is ~ 4000 . While alternative criteria are available (see Vynatheya et al. 2022 for a comparison of stability criteria as well as the most updated criteria), our systems are sufficiently far from the dynamical stability boundary that the detailed choice of criterion does not affect our result. Interestingly, for our adopted parameters, the condition for the validity of the double-averaged approximation ($P_{\text{out}} \ll t_{\text{ZLK}} j_{\text{in,min}}$ with P_{out} the outer orbital period), is a strictly weaker constraint than the dynamical stability condition.

Finally, for our mechanism, we require that $\epsilon_{\text{rot}} > 9/4$ to suppress eccentricity oscillations on the stellar phase, while we require that $\epsilon_{\text{GR}} \lesssim 1$ in order for eccentricity oscillations to gradually induce merger of the BBH. The combination of the four conditions listed above results in the parameter space shown in Fig. 7. While the parameter space satisfying all four requisite conditions is quite small, it is straightforward to dramatically expand the allowed parameter space by invoking other mechanisms to suppress ZLK oscillations on the stellar binary phase; we discuss this more below in Section 6. Note that for larger-mass SMBHs, the binary dissociation time is longer, but this is due to a lower stellar density which has an adverse effect on event rates.

6. SUMMARY AND DISCUSSION

6.1. Summary of Results

In this paper, we have studied the formation of merging binary black holes (BBHs) formed from stellar binaries in the vicinity of a supermassive black hole. We have shown that the combination of stellar and coupled spin-orbit evolution can give rise to unexpected correlations in the observed spin distributions of BBHs. To

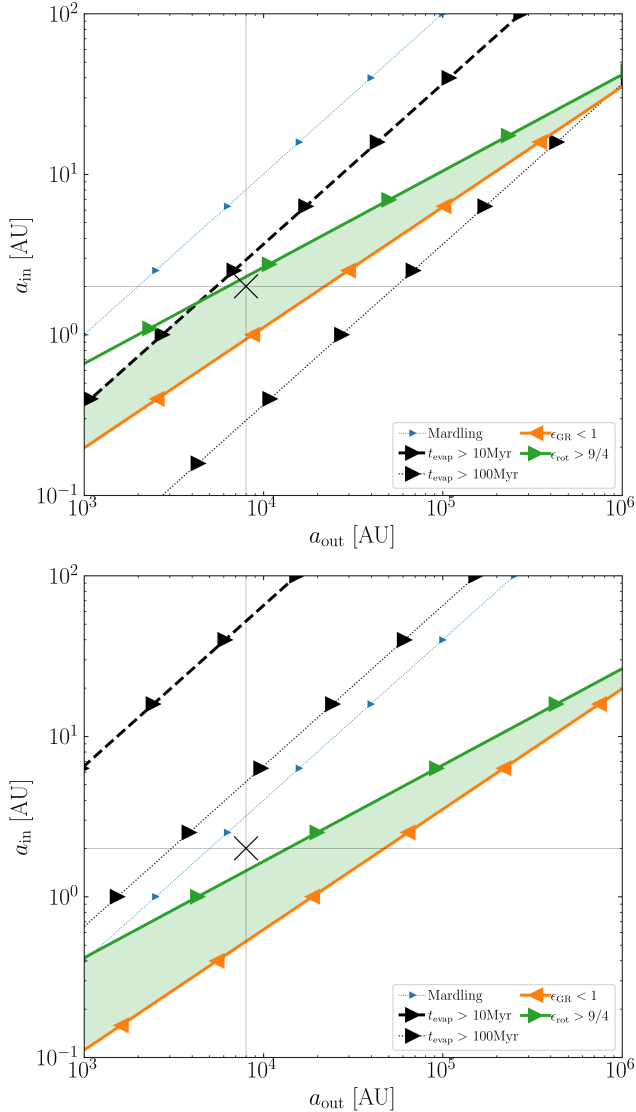


Figure 7. Parameter space available for the mechanism in this paper to form black hole binaries around a $10^7 M_\odot$ SMBH (top) and around a $10^8 M_\odot$ SMBH (bottom). The blue dotted line denotes the condition for dynamical instability (Eq. 61), the black dashed lines denote the condition for binary dissociation/evaporation timescale to be longer than 10 Myr and 100 Myr (Eq. 60), and the green and orange lines denote the required conditions on the SRFs in the system (Eqs. 51 and 53). The green shaded region denotes the region of parameter space satisfying all of our constraints. For simplicity, we hold a few parameters fixed: $m_{12,*} = 100 M_\odot$, $m_{12,\text{BH}} = 70 M_\odot$, $q_* = q_{\text{BH}} = 0.5$, $e_{\text{out}} = 0.6$, and we take $R_* = 10 R_\odot$ and $k_q = 0.02$, typical values for $\sim 60 M_\odot$ stars. The fiducial parameters used in this study are labeled by the horizontal and vertical dotted lines, located at $a_{\text{in}} = 2$ AU and $a_{\text{out}} = 8000$ AU = 0.04 pc.

be precise, the analytically tractable spin evolution of a BBH from formation to merger (Section 2, and Eq. 40) combines with the stellar evolution of the progenitor binary (Section 3) to yield a correlation between the mass ratio q and spin-orbit misalignment angles $\theta_{1,2}$ of the merging BBHs (Section 4 and Fig. 6). This correlation is reminiscent of the observed q - χ_{eff} correlation (Callister et al. 2021; Abbott et al. 2023; Callister 2024)³. Nevertheless, our work represents an important step in identifying possible sources of structure in the distribution of BH spins formed in gravitationally-driven BBH merger channels.

6.2. Discussion and Comparison to Other Mechanisms

We begin by reviewing the most recent results on the spin statistics as of the third Gravitational Wave Transient Catalog (GWTC-3 Abbott et al. 2023). First, it has now become clear that, while BH spins are still likely preferentially aligned with their orbits, this preference has weakened since GWTC-2 (Abbott et al. 2023; Callister 2024)—in fact, the distribution of θ is now marginally consistent with isotropy. More flexible statistical analyses uncover a tentative, statistically insignificant peak in the θ distribution around $\sim 60^\circ$, broadly consistent with our mechanism (Vitale et al. 2022; Edelman et al. 2023; Callister & Farr 2024; Baibhav & Kalogera 2024). On the other hand, the q - χ_{eff} correlation has strengthened with the full GWTC-3 catalog (Abbott et al. 2023), suggesting that this correlation reflects some substructure in the spin distributions (though more flexible models find a weaker correlation, Heinzl et al. 2024).

While the efficiency of the mechanism as presented is modest (Section 5), it also poses several advantages compared to existing mechanisms in the literature:

- Compared to previous studies of tertiary-induced mergers, our mechanism has a physical mechanism for the BBH’s initial spin-orbit alignment, namely the preceding MT phase. This primordial alignment is put in by fiat in existing studies of tertiary-driven mergers that report strongly-peaked spin distributions (Antonini et al. 2018; Liu & Lai 2018; Su et al. 2021a), and the spin-orbit misalignments become isotropic when these initial conditions are

³ Direct comparison of the two trends is complicated by the unknown BH spin magnitudes ($\chi_{1,2}$ in Eq. 1). These are expected to be slow based on theoretical arguments (Fuller & Ma 2019; Marchant et al. 2024), but other studies suggest more rapid rotation based on helioseismic constraints (Eggenberger et al. 2019), and inferences from the LVK data find $\chi \sim 0.2$ (Abbott et al. 2023).

not well-obeyed (Fragione & Kocsis 2020; Yu et al. 2020).

Näively, it would be expected that the orbital orientations of wider stellar binaries ($a_{\text{in}} \gtrsim 100$ AU) likely have no correlation with the stellar spin directions due to the vast difference in spatial scales. However, recent observations of exoplanetary systems suggest that the spins of stars may sometimes be aligned with the orbital planes of their binary companions out to several hundreds of AU, likely as a consequence of their formation (Rice et al. 2024). As such, we can speculate that the assumption of initial spin alignment in previous studies may be somewhat justified.

Our work also differs from studies where the tertiary is a stellar-mass companion. In such systems, the octupole-order effects in the hierarchical expansion (Eq. 10) are much stronger and more efficiently produce extreme eccentricities in BBHs with unequal mass ratios (Ford et al. 2000; Naoz 2016; Silsbee & Tremaine 2017). Some studies find that such an enhancement is incompatible with LVK data (Su et al. 2021b), though comparison with other studies suggests that this conclusion may be dependent on the inner binary separation (Martinez et al. 2022). When the tertiary is an SMBH, the octupole-order effects are much weaker due to the large value of a_{out} (Eq. 13).

Finally, a common obstacle in tertiary-induced mergers is modification (and even unbinding) of the inner and outer orbits during BH formation, both due to natal kicks and Blaauw kicks (e.g. Fragione & Kocsis 2020; Liu & Lai 2021; Su et al. 2024). In our mechanism, the large Kelperian orbital velocities of both the inner and outer orbits ($v_{\text{in}} \sim 200$ km/s and $v_{\text{out}} \sim 10^3$ km/s) allow us to neglect the effect of natal kicks during the formation of the BHs (which are poorly constrained but are typically assumed to be $\lesssim 100$ km/s if not substantially lower, e.g. Rodriguez et al. 2016).

- Compared to formation channels where BBH are dynamically assembled, our channel provides mechanisms for introducing preferred spin orientations (via MT) and matching the correlations found in the LVK observations. The spins of BHs in dynamically assembled binaries are typically thought to isotropically oriented at formation (Costa et al. 2023), leading to a uniform distribution of $\cos\theta$ (and a triangular distribution in χ_{eff} , Fragione & Kocsis 2020). Note that late-stage general relativistic effects can drive the in-plane com-

ponents of BH spins from isotropy towards [anti]alignment (Schnittman 2004; Gerosa et al. 2013, 2023), but this does not affect χ_{eff} . However, recent work suggests that BBHs in dense stellar environments may have their component spins realigned with their orbits if they experience collisions with nearby stars (Kiroglu et al. 2025).

- Compared to BBH formation via isolated binary evolution, our mechanism does not require rather precise amounts of orbital shrinkage via a common envelope phase. The stellar binaries we consider experience only moderate orbital evolution during their two phases of stable MT. On the other hand, recent works suggest that the LVK spin signatures, including the q - χ_{eff} correlation, may be reproducible with isolated binary evolution alone (Olejak et al. 2024; Banerjee & Olejak 2024; Baibhav & Kalogera 2024).
- Compared to BBH formation and merging in the disks of active galactic nuclei (AGN), our mechanism is less sensitive to the details of the local environment and highly uncertain hydrodynamical effects (see Lai & Muñoz 2023, for a recent review). Nevertheless, the AGN channel currently provides many prospects for reproducing the observed spin signatures as well as the high-mass end of merging BBH systems, and its detailed quantitative predictions are still being better understood (e.g. Li et al. 2021; Wang et al. 2021; McKernan et al. 2022; Santini et al. 2023; Cook et al. 2024). Moreover, if indeed SMBHs grow due to episodic bursts of accretion from AGN disks that persist only for a characteristic lifetime ~ 0.1 Myr (as suggested by Schawinski et al. 2015), the gas-free dynamics explored in this work and the AGN disk-driven may be alternatively active in driving BBH mergers in NSC.

Finally, it must be noted that the entire LVK catalog may arise from multiple formation channels, and recent work presents tentative evidence towards this possibility in the spin and mass ratio signatures (Zevin et al. 2021; Kimball et al. 2021; Li et al. 2024b,a; Hussain et al. 2024; Li et al. 2025).

6.3. Caveats and Future Work

Due to the broad scope of our work and the approximate treatments contained within it, there are numerous caveats and avenues for future work. We group this discussion in approximate correspondance to the sections as presented in the main text.

First, we discuss the details of the spin and orbital evolution. In expanding the interaction potential to octupole order and performing a double averaging over the inner and outer orbits, we have neglected terms of the hexadecapole order and higher (Will 2017, 2021; Conway & Will 2024) as well as neglected effects due to the breakdown of the outer orbit’s averaging (Luo et al. 2016; Grishin et al. 2018). For the extreme orbital hierarchies we consider ($a_{\text{in}}/a_{\text{out}} \sim P_{\text{in}}/P_{\text{out}} \lesssim 10^{-3}$), both of these approximations are well-justified: indeed, the evolution is dominated by the quadrupole-order ZLK evolution, and both the octupole-order and Brown’s Hamiltonians already only contribute negligibly. However, if the spin dynamics considered in this work and preceding ones (Liu & Lai 2018; Su et al. 2021a) is to be extended to lower-mass tertiary companions or to other regions of the nuclear star cluster where these effects are not so negligible, the spin adiabatic invariant must be quantitatively re-examined, as the ZLK cycles are no longer sufficiently regular to justify the assumptions of Section 2.2. Generally, as these higher-order effects become marginally important, one expects conservation of the adiabatic invariant θ_{eff} (Eq. 40) to become poorer, broadening the resulting θ distribution without significant effects to the mean (e.g. Fig. 20 of Liu & Lai 2018).

Next, we discuss our treatment of binary stellar evolution (BSE). Note that, the many simplifying assumptions we have made notwithstanding, the key objective with our evolution was to determine the strength of any correlation between the BBH’s initial semi-major axis and mass ratio. We encourage investigation of such correlations with more sophisticated BSE models, in particular with modern binary evolution codes such as POSYDON (Fragos et al. 2023; Andrews et al. 2024) that correctly capture the double mass transfer we invoke (as opposed to older codes based on Hurley et al. 2002 that likely overpredict the onset of common envelope evolution, e.g. Gallegos-Garcia et al. 2021). Even so, we discuss some uncertainties in our parameter choices below. First, we have chosen a moderate amount of wind-powered mass loss ($\eta_{\text{wind}} = 0.2$) reflecting the recent prevailing wisdom that winds are likely subdominant to binary mass transfer in stripping massive stars (Smith 2014; Vinciguerra et al. 2020). On the other hand, η_{wind} is likely larger for higher-metallicity stars, and the mean metallicity in the Milky Way’s NSC appears to solar to super-solar (Lépine et al. 2011; Do et al. 2015; Schödel, R. et al. 2020), so we have chosen not to fully neglect it. The details of whether MT in a binary is stable or unstable are uncertain, and likely depend on both mass ratio and orbital separation (e.g. Schneider et al. 2015; Schürmann & Langer 2024) as well as the specifics of

stellar evolution (e.g. Passy et al. 2012; Pavlovskii & Ivanova 2015; Agrawal et al. 2020; Klencki, Jakub et al. 2022; Temmink, K. D. et al. 2023). Furthermore, note that while our adopted accretion efficiency during the first stable MT phase ($\epsilon_2 = 0.5$) is standard (Meurs & van den Heuvel 1989; Dominik et al. 2012; van Son et al. 2022; Schürmann & Langer 2024), the most physical values for ϵ_2 may be substantially smaller if rotationally-enhanced stellar winds efficiently re-emit material from the accretor during the MT phase (Paxton et al. 2015; Andrews et al. 2024, but see Vinciguerra et al. 2020). Additionally, ϵ_2 may vary as a function of mass ratio (e.g. Schneider et al. 2015). Nevertheless, Fig. 4 suggests that the correlation we seek may be relatively insensitive to these uncertainties considered above. Finally, our neglect of BH natal kicks was made under the assumption that the kick velocities are $\lesssim 100$ km/s, in agreement with both standard population synthesis prescriptions (Rodriguez et al. 2016; Giacobbo & Mapelli 2020) and recent observational constraints (Kimball et al. 2023; Vigna-Gómez et al. 2024; Banagiri et al. 2023; Burdge et al. 2024).

One assumption made in this work, for simplicity, is a unimodal initial stellar semi-major axis distribution $a_{\text{in},\star}$. While certainly oversimplified, a preferred semi-major axis for BBH progenitors may be well-justified: compact binaries experience strong SRFs that suppress ZLK oscillations, while wide binaries can merge on the main sequence after reaching sufficiently high eccentricities (e.g. Stephan et al. 2016; Leigh et al. 2016; Fragione & Antonini 2019). Furthermore, star formation is thought not to be particularly efficient at \lesssim AU scales (Offner et al. 2023), introducing another characteristic scale to the $a_{\text{in},\star}$ distribution. Nevertheless, comparative studies with different $a_{\text{in},\star}$ distributions should certainly be incorporated before quantitative comparisons to observation are made, which we defer to future work.

Finally, we discuss the uncertainties regarding the feasibility of our mechanism in galactic center environments. While the formation of NSCs remains an open question (being primarily attributed to either infalling globular clusters or in situ formation, see Neumayer et al. 2020 for a recent review), the young inferred age of stars in the Milky Way NSC (Figer et al. 2004; Rossa et al. 2006; Do et al. 2015) and several observed binaries near Sgr A* (Martins et al. 2006; Pfuhl et al. 2014; Peißker et al. 2024, with parameters similar to our fiducial ones) suggest that there may be a continually-replenished population of massive stellar binaries like those considered in this work (but see also Chu et al. 2023).

It is worth noting that, in the dense stellar environments of NSCs, a key constraint of the mechanism as proposed in this work can be relaxed. The small parameter space shown in Fig. 7 is most strongly constrained by the requirement that the primordial stellar binary avoid ZLK via strong SRFs, while the resulting BBH merges efficiently via ZLK-driven eccentricity oscillation. We made this choice in order to most clearly illustrate the properties of the BH spin distributions that can result from our mechanism. However, it can instead be the case that the initial stellar binary is either initially compact or aligned with the outer orbit, and relaxation effects drive the binary into a ZLK-active configuration. This can be either due to two-body relaxation that softens the binary orbit (e.g. Collins & Sari 2008; Naoz et al. 2022; Winter-Granic et al. 2024; Hamilton & Modak 2024) or due to resonant relaxation (Rauch & Tremaine 1996; Hamers et al. 2018). We defer the inclusion of these effects to future work, as the impulsive nature of each successive close encounter likely complicates the spin evolution of the BBH components, broadening their observed distributions but potentially

retaining some fundamental correlation driven by the mechanism introduced here.

1 YS thanks Lieke van Son for many long discussions
2 about the intricacies of binary evolution. YS also
3 thanks Mark Dodici, Will Farr, Saavik Ford, Evgeny Gr-
4 ishin, Vicky Kalogera, Barry McKernan, Dong Lai, Bin
5 Liu, Shaunak Modak, Carl Rodriguez, Connor Rowan,
6 Mor Rozner, Eliot Quataert, Lucas M. de Sá, and
7 Sylvia Biscoveanu for helpful comments. This work
8 used the San Diego Supercomputer Center through al-
9 location PHY230201 from the Advanced Cyberinfras-
10 tructure Coordination Ecosystem: Services & Support
11 (ACCESS) program, which is supported by U.S. Na-
12 tional Science Foundation grants #2138259, #2138286,
13 #2138307, #2137603, and #2138296.

Software: Numpy (Harris et al. 2020), Scipy (Vir-
tanen et al. 2020), Matplotlib (Hunter 2007), Sympy
(Meurer et al. 2017), Astropy (Astropy Collaboration
et al. 2013), MESA (Paxton et al. 2011, 2013, 2015, 2018,
2019; Jermyn et al. 2023).

REFERENCES

- Abbott, R., Abe, H., Acernese, F., et al. 2023, ApJS, 267, 29, doi: [10.3847/1538-4365/acdc9f](https://doi.org/10.3847/1538-4365/acdc9f)
- Agrawal, P., Hurley, J., Stevenson, S., Szécsi, D., & Flynn, C. 2020, MNRAS, 497, 4549, doi: [10.1093/mnras/staa2264](https://doi.org/10.1093/mnras/staa2264)
- Alexander, M. 1973, Astrophysics and Space Science, 23, 459
- Alexander, T. 2017, ARA&A, 55, 17, doi: [10.1146/annurev-astro-091916-055306](https://doi.org/10.1146/annurev-astro-091916-055306)
- Ali, B., Paul, D., Eckart, A., et al. 2020, ApJ, 896, 100, doi: [10.3847/1538-4357/ab93ae](https://doi.org/10.3847/1538-4357/ab93ae)
- Andrews, J. J., Bavera, S. S., Briel, M., et al. 2024, arXiv e-prints, arXiv:2411.02376, doi: [10.48550/arXiv.2411.02376](https://doi.org/10.48550/arXiv.2411.02376)
- Antonini, F., Faber, J., Gualandris, A., & Merritt, D. 2010, ApJ, 713, 90, doi: [10.1088/0004-637X/713/1/90](https://doi.org/10.1088/0004-637X/713/1/90)
- Antonini, F., Murray, N., & Mikkola, S. 2014, ApJ, 781, 45, doi: [10.1088/0004-637x/781/1/45](https://doi.org/10.1088/0004-637x/781/1/45)
- Antonini, F., & Perets, H. B. 2012a, ApJ, 757, 27, doi: [10.1088/0004-637x/757/1/27](https://doi.org/10.1088/0004-637x/757/1/27)
- . 2012b, ApJ, 757, 27, doi: [10.1088/0004-637X/757/1/27](https://doi.org/10.1088/0004-637X/757/1/27)
- Antonini, F., & Rasio, F. A. 2016, ApJ, 831, 187, doi: [10.3847/0004-637X/831/2/187](https://doi.org/10.3847/0004-637X/831/2/187)
- Antonini, F., Rodriguez, C. L., Petrovich, C., & Fischer, C. L. 2018, MNRAS: Letters, 480, L58
- Antonini, F., Toonen, S., & Hamers, A. S. 2017, ApJ, 841, 77, doi: [10.3847/1538-4357/aa6f5e](https://doi.org/10.3847/1538-4357/aa6f5e)
- Arca Sedda, M., Mapelli, M., Benacquista, M., & Spera, M. 2023, MNRAS, 520, 5259, doi: [10.1093/mnras/stad331](https://doi.org/10.1093/mnras/stad331)
- Astropy Collaboration, Robitaille, T. P., Tollerud, E. J., et al. 2013, A&A, 558, A33, doi: [10.1051/0004-6361/201322068](https://doi.org/10.1051/0004-6361/201322068)
- Bahcall, J. N., & Wolf, R. A. 1976, ApJ, 209, 214, doi: [10.1086/154711](https://doi.org/10.1086/154711)
- Baibhav, V., & Kalogera, V. 2024, arXiv e-prints, arXiv:2412.03461, doi: [10.48550/arXiv.2412.03461](https://doi.org/10.48550/arXiv.2412.03461)
- Banagiri, S., Doctor, Z., Kalogera, V., Kimball, C., & Andrews, J. J. 2023, ApJ, 959, 106, doi: [10.3847/1538-4357/ad0557](https://doi.org/10.3847/1538-4357/ad0557)
- Banerjee, S., Baumgardt, H., & Kroupa, P. 2010, MNRAS, 402, 371, doi: [10.1111/j.1365-2966.2009.15880.x](https://doi.org/10.1111/j.1365-2966.2009.15880.x)
- Banerjee, S., & Olejak, A. 2024, arXiv e-prints, arXiv:2411.15112, doi: [10.48550/arXiv.2411.15112](https://doi.org/10.48550/arXiv.2411.15112)
- Barber, J., & Antonini, F. 2024, arXiv e-prints, arXiv:2410.03832, doi: [10.48550/arXiv.2410.03832](https://doi.org/10.48550/arXiv.2410.03832)
- Barker, B. M., & O’Connell, R. F. 1975, PhRvD, 12, 329, doi: [10.1103/PhysRevD.12.329](https://doi.org/10.1103/PhysRevD.12.329)
- Bartos, I., Kocsis, B., Haiman, Z., & Márka, S. 2017, ApJ, 835, 165, doi: [10.3847/1538-4357/835/2/165](https://doi.org/10.3847/1538-4357/835/2/165)
- Belczynski, K., Dominik, M., Bulik, T., et al. 2010, ApJL, 715, L138, doi: [10.1088/2041-8205/715/2/L138](https://doi.org/10.1088/2041-8205/715/2/L138)

- Belczynski, K., Holz, D. E., Bulik, T., & O’Shaughnessy, R. 2016, *Nature*, 534, 512
- Belczynski, K., Klencki, J., Fields, C. E., et al. 2020, *A&A*, 636, A104, doi: [10.1051/0004-6361/201936528](https://doi.org/10.1051/0004-6361/201936528)
- Binney, J., & Tremaine, S. 2008, *Galactic Dynamics: Second Edition* (Princeton University Press)
- Braun, H., & Langer, N. 1995, *A&A*, 297, 483
- Bruel, T., Rodriguez, C. L., Lamberts, A., et al. 2024, *A&A*, 686, A106, doi: [10.1051/0004-6361/202348716](https://doi.org/10.1051/0004-6361/202348716)
- Burdge, K. B., El-Badry, K., Kara, E., et al. 2024, arXiv e-prints, arXiv:2404.03719
- Callister, T. A. 2024, arXiv e-prints, arXiv:2410.19145, doi: [10.48550/arXiv.2410.19145](https://doi.org/10.48550/arXiv.2410.19145)
- Callister, T. A., & Farr, W. M. 2024, *Physical Review X*, 14, 021005, doi: [10.1103/PhysRevX.14.021005](https://doi.org/10.1103/PhysRevX.14.021005)
- Callister, T. A., Haster, C.-J., Ng, K. K. Y., Vitale, S., & Farr, W. M. 2021, *ApJL*, 922, L5, doi: [10.3847/2041-8213/ac2ccc](https://doi.org/10.3847/2041-8213/ac2ccc)
- Chattopadhyay, D., Stegmann, J., Antonini, F., Barber, J., & Romero-Shaw, I. M. 2023, *MNRAS*, 526, 4908, doi: [10.1093/mnras/stad3048](https://doi.org/10.1093/mnras/stad3048)
- Choi, J., Dotter, A., Conroy, C., et al. 2016, *ApJ*, 823, 102, doi: [10.3847/0004-637X/823/2/102](https://doi.org/10.3847/0004-637X/823/2/102)
- Chu, D. S., Do, T., Ghez, A., et al. 2023, *ApJ*, 948, 94, doi: [10.3847/1538-4357/acc93e](https://doi.org/10.3847/1538-4357/acc93e)
- Collins, B. F., & Sari, R. 2008, *ApJ*, 136, 2552, doi: [10.1088/0004-6256/136/6/2552](https://doi.org/10.1088/0004-6256/136/6/2552)
- Conway, L., & Will, C. M. 2024, *PhRvD*, 110, 083022, doi: [10.1103/PhysRevD.110.083022](https://doi.org/10.1103/PhysRevD.110.083022)
- Cook, H. E., McKernan, B., Ford, K. E. S., et al. 2024, arXiv e-prints, arXiv:2411.10590, doi: [10.48550/arXiv.2411.10590](https://doi.org/10.48550/arXiv.2411.10590)
- Costa, G., Chruślińska, M., Klencki, J., et al. 2023, arXiv e-prints, arXiv:2311.15778, doi: [10.48550/arXiv.2311.15778](https://doi.org/10.48550/arXiv.2311.15778)
- De, K., MacLeod, M., Jencson, J. E., et al. 2024, arXiv e-prints, arXiv:2410.14778, doi: [10.48550/arXiv.2410.14778](https://doi.org/10.48550/arXiv.2410.14778)
- De Mink, S., & Mandel, I. 2016, *MNRAS*, 460, 3545
- Do, T., Kerzendorf, W., Winsor, N., et al. 2015, *ApJ*, 809, 143, doi: [10.1088/0004-637X/809/2/143](https://doi.org/10.1088/0004-637X/809/2/143)
- Dominik, M., Belczynski, K., Fryer, C., et al. 2012, *ApJ*, 759, 52
- Dotter, A. 2016, *ApJS*, 222, 8, doi: [10.3847/0067-0049/222/1/8](https://doi.org/10.3847/0067-0049/222/1/8)
- Downing, J., Benacquista, M., Giersz, M., & Spurzem, R. 2010, *MNRAS*, 407, 1946
- Edelman, B., Farr, B., & Doctor, Z. 2023, *ApJ*, 946, 16, doi: [10.3847/1538-4357/acb5ed](https://doi.org/10.3847/1538-4357/acb5ed)
- Eggenberger, P., Buldgen, G., & Salmon, S. J. A. J. 2019, *A&A*, 626, L1, doi: [10.1051/0004-6361/201935509](https://doi.org/10.1051/0004-6361/201935509)
- Eggleton, P. P., & Kiseleva-Eggleton, L. 2001, *ApJ*, 562, 1012, doi: [10.1086/323843](https://doi.org/10.1086/323843)
- Figer, D. F., Rich, R. M., Kim, S. S., Morris, M., & Serabyn, E. 2004, *ApJ*, 601, 319, doi: [10.1086/380392](https://doi.org/10.1086/380392)
- Ford, E. B., Kozinsky, B., & Rasio, F. A. 2000, *ApJ*, 535, 385
- Fornasini, F., Antoniou, V., & Dubus, G. 2024, in *Handbook of X-ray and Gamma-ray Astrophysics* (Springer), 3719–3773
- Fragione, G., & Antonini, F. 2019, *MNRAS*, 488, 728, doi: [10.1093/mnras/stz1723](https://doi.org/10.1093/mnras/stz1723)
- Fragione, G., Grishin, E., Leigh, N. W. C., Perets, H. B., & Perna, R. 2019, *MNRAS*, 488, 47, doi: [10.1093/mnras/stz1651](https://doi.org/10.1093/mnras/stz1651)
- Fragione, G., & Kocsis, B. 2020, *MNRAS*, 493, 3920, doi: [10.1093/mnras/staa443](https://doi.org/10.1093/mnras/staa443)
- Fragione, G., & Loeb, A. 2019, *MNRAS*, 486, 4443
- Fragos, T., Andrews, J. J., Bavera, S. S., et al. 2023, *ApJS*, 264, 45, doi: [10.3847/1538-4365/ac90c1](https://doi.org/10.3847/1538-4365/ac90c1)
- Fuller, J., & Ma, L. 2019, *ApJL*, 881, L1
- Gallego-Cano, E., Schödel, R., Dong, H., et al. 2018, *A&A*, 609, A26, doi: [10.1051/0004-6361/201730451](https://doi.org/10.1051/0004-6361/201730451)
- Gallegos-Garcia, M., Berry, C. P. L., Marchant, P., & Kalogera, V. 2021, *ApJ*, 922, 110, doi: [10.3847/1538-4357/ac2610](https://doi.org/10.3847/1538-4357/ac2610)
- Gerosa, D., Fumagalli, G., Mould, M., et al. 2023, *PhRvD*, 108, 024042, doi: [10.1103/PhysRevD.108.024042](https://doi.org/10.1103/PhysRevD.108.024042)
- Gerosa, D., Kesden, M., Berti, E., O’Shaughnessy, R., & Sperhake, U. 2013, *PhRvD*, 87, 104028, doi: [10.1103/PhysRevD.87.104028](https://doi.org/10.1103/PhysRevD.87.104028)
- Giacobbo, N., & Mapelli, M. 2020, *ApJ*, 891, 141, doi: [10.3847/1538-4357/ab7335](https://doi.org/10.3847/1538-4357/ab7335)
- Gondán, L., Kocsis, B., Raffai, P., & Frei, Z. 2018, *ApJ*, 860, 5
- Grishin, E. 2024, *MNRAS*, 533, 486, doi: [10.1093/mnras/stae1833](https://doi.org/10.1093/mnras/stae1833)
- Grishin, E., & Perets, H. B. 2022, *MNRAS*, 512, 4993, doi: [10.1093/mnras/stac706](https://doi.org/10.1093/mnras/stac706)
- Grishin, E., Perets, H. B., & Fragione, G. 2018, *MNRAS*, 481, 4907, doi: [10.1093/mnras/sty2477](https://doi.org/10.1093/mnras/sty2477)
- Hamers, A. S., Bar-Or, B., Petrovich, C., & Antonini, F. 2018, *ApJ*, 865, 2, doi: [10.3847/1538-4357/aadae2](https://doi.org/10.3847/1538-4357/aadae2)
- Hamilton, C., & Modak, S. 2024, *MNRAS*, 532, 2425, doi: [10.1093/mnras/stae1654](https://doi.org/10.1093/mnras/stae1654)
- Harris, C. R., Millman, K. J., van der Walt, S. J., et al. 2020, *Nature*, 585, 357
- Heinzel, J., Vitale, S., & Biscoveanu, S. 2024, *PhRvD*, 109, 103006, doi: [10.1103/PhysRevD.109.103006](https://doi.org/10.1103/PhysRevD.109.103006)

- Hellings, P. 1983, *Ap&SS*, 96, 37, doi: [10.1007/BF00661941](https://doi.org/10.1007/BF00661941)
- Hoang, B.-M., Naoz, S., Kocsis, B., Rasio, F. A., & Dosopoulou, F. 2018, *ApJ*, 856, 140
- Hunter, J. D. 2007, *Computing in Science and Engineering*, 9, 90
- Hurley, J. R., Tout, C. A., & Pols, O. R. 2002, *MNRAS*, 329, 897, doi: [10.1046/j.1365-8711.2002.05038.x](https://doi.org/10.1046/j.1365-8711.2002.05038.x)
- Hussain, A., Isi, M., & Zimmerman, A. 2024, arXiv e-prints, arXiv:2411.02252, doi: [10.48550/arXiv.2411.02252](https://doi.org/10.48550/arXiv.2411.02252)
- Hut, P. 1981, *A&A*, 99, 126
- Hut, P. 1985, in *IAU Symposium*, Vol. 113, *Dynamics of Star Clusters*, ed. J. Goodman & P. Hut, 231–247
- Jermyn, A. S., Bauer, E. B., Schwab, J., et al. 2023, *ApJS*, 265, 15, doi: [10.3847/1538-4365/acae8d](https://doi.org/10.3847/1538-4365/acae8d)
- Johnston, C. 2021, *A&A*, 655, A29, doi: [10.1051/0004-6361/202141080](https://doi.org/10.1051/0004-6361/202141080)
- Jurado, C., Naoz, S., Lam, C. Y., & Hoang, B.-M. 2024, *ApJ*, 971, 95, doi: [10.3847/1538-4357/ad55ee](https://doi.org/10.3847/1538-4357/ad55ee)
- Kimball, C., Talbot, C., Berry, C. P. L., et al. 2021, *ApJL*, 915, L35, doi: [10.3847/2041-8213/ac0aef](https://doi.org/10.3847/2041-8213/ac0aef)
- Kimball, C., Imperato, S., Kalogera, V., et al. 2023, *ApJL*, 952, L34, doi: [10.3847/2041-8213/ace526](https://doi.org/10.3847/2041-8213/ace526)
- Kiroğlu, F., Lombardi, Jr., J. C., Kremer, K., Vanderzyden, H. D., & Rasio, F. A. 2025, arXiv e-prints, arXiv:2501.09068, doi: [10.48550/arXiv.2501.09068](https://doi.org/10.48550/arXiv.2501.09068)
- Kiseleva, L. G., Eggleton, P. P., & Mikkola, S. 1998, *MNRAS*, 300, 292, doi: [10.1046/j.1365-8711.1998.01903.x](https://doi.org/10.1046/j.1365-8711.1998.01903.x)
- Klencki, Jakub, Istrate, Alina, Nelemans, Gijs, & Pols, Onno. 2022, *A&A*, 662, A56, doi: [10.1051/0004-6361/202142701](https://doi.org/10.1051/0004-6361/202142701)
- Kozai, Y. 1962, *AJ*, 67, 591
- Lai, D. 2012, *MNRAS*, 423, 486, doi: [10.1111/j.1365-2966.2012.20893.x](https://doi.org/10.1111/j.1365-2966.2012.20893.x)
- Lai, D., & Muñoz, D. J. 2023, *ARA&A*, 61, 517, doi: [10.1146/annurev-astro-052622-022933](https://doi.org/10.1146/annurev-astro-052622-022933)
- Landau, L. D., & Lifshitz, E. M. 1969, *Mechanics* (Wesley Publishing Company, Inc., Reading, Massachusetts)
- Leigh, N. W., Geller, A. M., McKernan, B., et al. 2018, *MNRAS*, 474, 5672
- Leigh, N. W. C., Antonini, F., Stone, N. C., Shara, M. M., & Merritt, D. 2016, *MNRAS*, 463, 1605, doi: [10.1093/mnras/stw2018](https://doi.org/10.1093/mnras/stw2018)
- Lépine, J. R. D., Cruz, P., Scarano, S., J., et al. 2011, *MNRAS*, 417, 698, doi: [10.1111/j.1365-2966.2011.19314.x](https://doi.org/10.1111/j.1365-2966.2011.19314.x)
- Li, J., Lai, D., & Rodet, L. 2022, *ApJ*, 934, 154, doi: [10.3847/1538-4357/ac7c0d](https://doi.org/10.3847/1538-4357/ac7c0d)
- Li, R., & Lai, D. 2022, *MNRAS*, 517, 1602, doi: [10.1093/mnras/stac2577](https://doi.org/10.1093/mnras/stac2577)
- Li, Y.-J., Tang, S.-P., Gao, S.-J., Wu, D.-C., & Wang, Y.-Z. 2024a, *ApJ*, 977, 67, doi: [10.3847/1538-4357/ad83b5](https://doi.org/10.3847/1538-4357/ad83b5)
- Li, Y.-J., Wang, Y.-Z., Tang, S.-P., Chen, T., & Fan, Y.-Z. 2025, arXiv e-prints. <https://arxiv.org/abs/2501.09495>
- Li, Y.-J., Wang, Y.-Z., Tang, S.-P., & Fan, Y.-Z. 2024b, *PhRvL*, 133, 051401, doi: [10.1103/PhysRevLett.133.051401](https://doi.org/10.1103/PhysRevLett.133.051401)
- Li, Y.-P., Dempsey, A. M., Li, S., Li, H., & Li, J. 2021, *ApJ*, 911, 124, doi: [10.3847/1538-4357/abed48](https://doi.org/10.3847/1538-4357/abed48)
- Lidov, M. L. 1962, *Planetary and Space Science*, 9, 719
- Lipunov, V., Postnov, K., & Prokhorov, M. 1997, *Astronomy Letters*, 23, 492
- Liu, B., & Lai, D. 2017, *ApJL*, 846, L11
- . 2018, *ApJ*, 863, 68
- Liu, B., & Lai, D. 2019, *MNRAS*, 483, 4060, doi: [10.1093/mnras/sty3432](https://doi.org/10.1093/mnras/sty3432)
- . 2020, *PhRvD*, 102, 023020, doi: [10.1103/PhysRevD.102.023020](https://doi.org/10.1103/PhysRevD.102.023020)
- Liu, B., & Lai, D. 2021, *MNRAS*, 502, 2049
- Liu, B., Lai, D., & Wang, Y.-H. 2019a, *ApJ*, 881, 41, doi: [10.3847/1538-4357/ab2dfb](https://doi.org/10.3847/1538-4357/ab2dfb)
- . 2019b, *ApJL*, 883, L7, doi: [10.3847/2041-8213/ab40c0](https://doi.org/10.3847/2041-8213/ab40c0)
- Liu, B., Muñoz, D. J., & Lai, D. 2015a, *MNRAS*, 447, 747
- . 2015b, *MNRAS*, 447, 747, doi: [10.1093/mnras/stu2396](https://doi.org/10.1093/mnras/stu2396)
- Lu, W., Fuller, J., Quataert, E., & Bonnerot, C. 2023, *MNRAS*, 519, 1409, doi: [10.1093/mnras/stac3621](https://doi.org/10.1093/mnras/stac3621)
- Luo, L., Katz, B., & Dong, S. 2016, *MNRAS*, 458, 3060, doi: [10.1093/mnras/stw475](https://doi.org/10.1093/mnras/stw475)
- Mandel, I., & De Mink, S. E. 2016, *MNRAS*, 458, 2634
- Marchant, P., & Bodensteiner, J. 2024, *ARA&A*, 62, 21, doi: [10.1146/annurev-astro-052722-105936](https://doi.org/10.1146/annurev-astro-052722-105936)
- Marchant, P., Langer, N., Podsiadlowski, P., Tauris, T. M., & Moriya, T. J. 2016, *A&A*, 588, A50
- Marchant, P., Podsiadlowski, P., & Mandel, I. 2024, *A&A*, 691, A339, doi: [10.1051/0004-6361/202348190](https://doi.org/10.1051/0004-6361/202348190)
- Mardling, R. A., & Aarseth, S. J. 2001, *MNRAS*, 321, 398
- Martinez, M. A. S., Rodriguez, C. L., & Fragione, G. 2022, *ApJ*, 937, 78, doi: [10.3847/1538-4357/ac8d55](https://doi.org/10.3847/1538-4357/ac8d55)
- Martins, F., Trippe, S., Paumard, T., et al. 2006, *ApJL*, 649, L103, doi: [10.1086/508328](https://doi.org/10.1086/508328)
- McKernan, B., Ford, K. E. S., Callister, T., et al. 2022, *MNRAS*, 514, 3886, doi: [10.1093/mnras/stac1570](https://doi.org/10.1093/mnras/stac1570)
- McKernan, B., Ford, K. E. S., Cook, H. E., et al. 2024, arXiv e-prints, arXiv:2410.16515, doi: [10.48550/arXiv.2410.16515](https://doi.org/10.48550/arXiv.2410.16515)
- McKernan, B., Ford, K. E. S., Lyra, W., & Perets, H. B. 2012, *MNRAS*, 425, 460, doi: [10.1111/j.1365-2966.2012.21486.x](https://doi.org/10.1111/j.1365-2966.2012.21486.x)
- Meurer, A., Smith, C. P., Paprocki, M., et al. 2017, *PeerJ Computer Science*, 3, e103
- Meurs, E. J. A., & van den Heuvel, E. P. J. 1989, *A&A*, 226, 88

- Michaely, E., & Perets, H. B. 2020, *MNRAS*, 498, 4924, doi: [10.1093/mnras/staa2720](https://doi.org/10.1093/mnras/staa2720)
- Miller, M. C., & Hamilton, D. P. 2002, *ApJ*, 576, 894
- Miller, M. C., & Lauburg, V. M. 2009, *ApJ*, 692, 917
- Naoz, S. 2016, *ARAA*, 54, 441
- Naoz, S., Rose, S. C., Michaely, E., et al. 2022, *ApJL*, 927, L18, doi: [10.3847/2041-8213/ac574b](https://doi.org/10.3847/2041-8213/ac574b)
- Neumayer, N., Seth, A., & Böker, T. 2020, *A&A Rv*, 28, 4, doi: [10.1007/s00159-020-00125-0](https://doi.org/10.1007/s00159-020-00125-0)
- Offner, S. S. R., Moe, M., Kratter, K. M., et al. 2023, in *Astronomical Society of the Pacific Conference Series*, Vol. 534, *Protostars and Planets VII*, ed. S. Inutsuka, Y. Aikawa, T. Muto, K. Tomida, & M. Tamura, 275, doi: [10.48550/arXiv.2203.10066](https://doi.org/10.48550/arXiv.2203.10066)
- O’leary, R. M., Rasio, F. A., Fregeau, J. M., Ivanova, N., & O’Shaughnessy, R. 2006, *ApJ*, 637, 937
- Olejak, A., Klencki, J., Xu, X.-T., et al. 2024, *A&A*, 689, A305, doi: [10.1051/0004-6361/202450480](https://doi.org/10.1051/0004-6361/202450480)
- Passy, J.-C., Herwig, F., & Paxton, B. 2012, *ApJ*, 760, 90, doi: [10.1088/0004-637X/760/1/90](https://doi.org/10.1088/0004-637X/760/1/90)
- Pavlovskii, K., & Ivanova, N. 2015, *MNRAS*, 449, 4415, doi: [10.1093/mnras/stv619](https://doi.org/10.1093/mnras/stv619)
- Paxton, B., Bildsten, L., Dotter, A., et al. 2011, *ApJS*, 192, 3, doi: [10.1088/0067-0049/192/1/3](https://doi.org/10.1088/0067-0049/192/1/3)
- Paxton, B., Cantiello, M., Arras, P., et al. 2013, *ApJS*, 208, 4, doi: [10.1088/0067-0049/208/1/4](https://doi.org/10.1088/0067-0049/208/1/4)
- Paxton, B., Marchant, P., Schwab, J., et al. 2015, *ApJS*, 220, 15, doi: [10.1088/0067-0049/220/1/15](https://doi.org/10.1088/0067-0049/220/1/15)
- Paxton, B., Schwab, J., Bauer, E. B., et al. 2018, *ApJS*, 234, 34, doi: [10.3847/1538-4365/aaa5a8](https://doi.org/10.3847/1538-4365/aaa5a8)
- Paxton, B., Smolec, R., Schwab, J., et al. 2019, *ApJS*, 243, 10, doi: [10.3847/1538-4365/ab2241](https://doi.org/10.3847/1538-4365/ab2241)
- Pedersen, M. G., Aerts, C., Pápics, P. I., et al. 2021, *Nature Astronomy*, 5, 715, doi: [10.1038/s41550-021-01351-x](https://doi.org/10.1038/s41550-021-01351-x)
- Peißker, F., Zajaček, M., Labadie, L., et al. 2024, *Nature Communications*, 15, 10608, doi: [10.1038/s41467-024-54748-3](https://doi.org/10.1038/s41467-024-54748-3)
- Peters, P. C. 1964, *Phys. Rev.*, 136, B1224
- Pfuhl, O., Alexander, T., Gillessen, S., et al. 2014, *ApJ*, 782, 101, doi: [10.1088/0004-637X/782/2/101](https://doi.org/10.1088/0004-637X/782/2/101)
- Podsiadlowski, P., Rappaport, S., & Han, Z. 2003, *MNRAS*, 341, 385
- Portegies Zwart, S. F., & McMillan, S. L. W. 2000, *ApJL*, 528, L17, doi: [10.1086/312422](https://doi.org/10.1086/312422)
- Quinlan, G. D., & Shapiro, S. L. 1989, *ApJ*, 343, 725, doi: [10.1086/167745](https://doi.org/10.1086/167745)
- Racine, É. 2008, *PhRvD*, 78, 044021, doi: [10.1103/PhysRevD.78.044021](https://doi.org/10.1103/PhysRevD.78.044021)
- Randall, L., & Xianyu, Z.-Z. 2018, *ApJ*, 853, 93
- Rauch, K. P., & Tremaine, S. 1996, *NewA*, 1, 149, doi: [10.1016/S1384-1076\(96\)00012-7](https://doi.org/10.1016/S1384-1076(96)00012-7)
- Renzo, M., & Götzberg, Y. 2021, *ApJ*, 923, 277, doi: [10.3847/1538-4357/ac29c5](https://doi.org/10.3847/1538-4357/ac29c5)
- Rice, M., Gerbig, K., & Vanderburg, A. 2024, *AJ*, 167, 126, doi: [10.3847/1538-3881/ad1bed](https://doi.org/10.3847/1538-3881/ad1bed)
- Riley, J., Mandel, I., Marchant, P., et al. 2021, *MNRAS*, 505, 663
- Riley, J., Agrawal, P., Barrett, J. W., et al. 2022, *ApJS*, 258, 34, doi: [10.3847/1538-4365/ac416c](https://doi.org/10.3847/1538-4365/ac416c)
- Rodriguez, C. L., Amaro-Seoane, P., Chatterjee, S., & Rasio, F. A. 2018, *PhRvL*, 120, 151101
- Rodriguez, C. L., Chatterjee, S., & Rasio, F. A. 2016, *PhRvD*, 93, 084029
- Rodriguez, C. L., Morscher, M., Pattabiraman, B., et al. 2015, *PhRvL*, 115, 051101
- Rose, S. C., Naoz, S., Gautam, A. K., et al. 2020, *ApJ*, 904, 113, doi: [10.3847/1538-4357/abc557](https://doi.org/10.3847/1538-4357/abc557)
- Rossa, J., van der Marel, R. P., Böker, T., et al. 2006, *AJ*, 132, 1074, doi: [10.1086/505968](https://doi.org/10.1086/505968)
- Rowan, C., Boekholt, T., Kocsis, B., & Haiman, Z. 2023, *MNRAS*, 524, 2770, doi: [10.1093/mnras/stad1926](https://doi.org/10.1093/mnras/stad1926)
- Samsing, J., & D’Orazio, D. J. 2018, *MNRAS*, 481, 5445
- Samsing, J., & Ramirez-Ruiz, E. 2017, *ApJL*, 840, L14
- Samsing, J., Bartos, I., D’Orazio, D., et al. 2022, *Nature*, 603, 237
- Santini, A., Gerosa, D., Cotesta, R., & Berti, E. 2023, *PhRvD*, 108, 083033, doi: [10.1103/PhysRevD.108.083033](https://doi.org/10.1103/PhysRevD.108.083033)
- Schawinski, K., Koss, M., Berney, S., & Sartori, L. F. 2015, *MNRAS*, 451, 2517, doi: [10.1093/mnras/stv1136](https://doi.org/10.1093/mnras/stv1136)
- Schmidt, P., Ohme, F., & Hannam, M. 2015, *PhRvD*, 91, 024043
- Schneider, F. R. N., Izzard, R. G., Langer, N., & Mink, S. E. d. 2015, *ApJ*, 805, 20, doi: [10.1088/0004-637X/805/1/20](https://doi.org/10.1088/0004-637X/805/1/20)
- Schnittman, J. D. 2004, *PhRvD*, 70, 124020, doi: [10.1103/PhysRevD.70.124020](https://doi.org/10.1103/PhysRevD.70.124020)
- Schödel, R., Noguera-Lara, F., Gallego-Cano, E., et al. 2020, *A&A*, 641, A102, doi: [10.1051/0004-6361/201936688](https://doi.org/10.1051/0004-6361/201936688)
- Schürmann, C., & Langer, N. 2024, *A&A*, 691, A174, doi: [10.1051/0004-6361/202450354](https://doi.org/10.1051/0004-6361/202450354)
- Secunda, A., Bellovary, J., Mac Low, M.-M., et al. 2019, *ApJ*, 878, 85, doi: [10.3847/1538-4357/ab20ca](https://doi.org/10.3847/1538-4357/ab20ca)
- Silsbee, K., & Tremaine, S. 2017, *ApJ*, 836, 39
- Smith, N. 2014, *ARA&A*, 52, 487, doi: [https://doi.org/10.1146/annurev-astro-081913-040025](https://doi.org/https://doi.org/10.1146/annurev-astro-081913-040025)
- Soberman, G. E., Phinney, E. S., & van den Heuvel, E. P. J. 1997, *A&A*, 327, 620, doi: [10.48550/arXiv.astro-ph/9703016](https://doi.org/10.48550/arXiv.astro-ph/9703016)

- Steinle, N., & Kesden, M. 2021, *PhRvD*, 103, 063032, doi: [10.1103/PhysRevD.103.063032](https://doi.org/10.1103/PhysRevD.103.063032)
- Stephan, A. P., Naoz, S., Ghez, A. M., et al. 2016, *MNRAS*, 460, 3494, doi: [10.1093/mnras/stw1220](https://doi.org/10.1093/mnras/stw1220)
- Stone, N. C., Metzger, B. D., & Haiman, Z. 2017, *MNRAS*, 464, 946, doi: [10.1093/mnras/stw2260](https://doi.org/10.1093/mnras/stw2260)
- Su, Y., Lai, D., & Liu, B. 2021a, *PhRvD*, 103, 063040
- Su, Y., Liu, B., & Lai, D. 2021b, *MNRAS*, 505, 3681
- Su, Y., Liu, B., & Xu, S. 2024, *ApJ*, 971, 139
- Tagawa, H., Haiman, Z., & Kocsis, B. 2020, *ApJ*, 898, 25
- Temminck, K. D., Pols, O. R., Justham, S., Istrate, A. G., & Toonen, S. 2023, *A&A*, 669, A45, doi: [10.1051/0004-6361/202244137](https://doi.org/10.1051/0004-6361/202244137)
- Tkachenko, A., Pavlovski, K., Johnston, C., et al. 2020, *A&A*, 637, A60, doi: [10.1051/0004-6361/202037452](https://doi.org/10.1051/0004-6361/202037452)
- Toyouchi, D., Hotokezaka, K., Inayoshi, K., & Kuiper, R. 2024, *MNRAS*, 532, 4826, doi: [10.1093/mnras/stae1798](https://doi.org/10.1093/mnras/stae1798)
- Tremaine, S. 2023, *MNRAS*, 522, 937, doi: [10.1093/mnras/stad1029](https://doi.org/10.1093/mnras/stad1029)
- Tremaine, S., Touma, J., & Namouni, F. 2009, *AJ*, 137, 3706, doi: [10.1088/0004-6256/137/3/3706](https://doi.org/10.1088/0004-6256/137/3/3706)
- Tremaine, S., Gebhardt, K., Bender, R., et al. 2002, *ApJ*, 574, 740, doi: [10.1086/341002](https://doi.org/10.1086/341002)
- van Son, L. A. C., de Mink, S. E., Renzo, M., et al. 2022, *ApJ*, 940, 184, doi: [10.3847/1538-4357/ac9b0a](https://doi.org/10.3847/1538-4357/ac9b0a)
- Vigna-Gómez, A., Willcox, R., Tamborra, I., et al. 2024, *PhRvL*, 132, 191403, doi: [10.1103/PhysRevLett.132.191403](https://doi.org/10.1103/PhysRevLett.132.191403)
- Vinciguerra, S., Neijssel, C. J., Vigna-Gómez, A., et al. 2020, *Monthly Notices of the Royal Astronomical Society*, 498, 4705, doi: [10.1093/mnras/staa2177](https://doi.org/10.1093/mnras/staa2177)
- Virtanen, P., Gommers, R., Oliphant, T. E., et al. 2020, *Nature Methods*, 17, 261
- Vitale, S., Biscoveanu, S., & Talbot, C. 2022, *A&A*, 668, L2, doi: [10.1051/0004-6361/202245084](https://doi.org/10.1051/0004-6361/202245084)
- von Zeipel, H. 1910, *Astronomische Nachrichten*, 183, 345
- Vynatheya, P., Hamers, A. S., Mardling, R. A., & Bellinger, E. P. 2022, *MNRAS*, 516, 4146, doi: [10.1093/mnras/stac2540](https://doi.org/10.1093/mnras/stac2540)
- Wang, Y.-H., McKernan, B., Ford, S., et al. 2021, *ApJL*, 923, L23, doi: [10.3847/2041-8213/ac400a](https://doi.org/10.3847/2041-8213/ac400a)
- Wen, L. 2003, *ApJ*, 598, 419
- Whitehead, H., Rowan, C., Boeholt, T., & Kocsis, B. 2024, *MNRAS*, 531, 4656, doi: [10.1093/mnras/stae1430](https://doi.org/10.1093/mnras/stae1430)
- Will, C. M. 2017, *PhRvD*, 96, 023017, doi: [10.1103/PhysRevD.96.023017](https://doi.org/10.1103/PhysRevD.96.023017)
- . 2021, *PhRvD*, 103, 063003, doi: [10.1103/PhysRevD.103.063003](https://doi.org/10.1103/PhysRevD.103.063003)
- Winter-Granic, M., Petrovich, C., Peña-Donaire, V., & Hamilton, C. 2024, *ApJ*, 973, 53, doi: [10.3847/1538-4357/ad61e1](https://doi.org/10.3847/1538-4357/ad61e1)
- Wu, Y., & Murray, N. 2003, *ApJ*, 589, 605, doi: [10.1086/374598](https://doi.org/10.1086/374598)
- Yu, H., Ma, S., Giesler, M., & Chen, Y. 2020, *PhRvD*, 102, 123009, doi: [10.1103/PhysRevD.102.123009](https://doi.org/10.1103/PhysRevD.102.123009)
- Zevin, M., Bavera, S. S., Berry, C. P. L., et al. 2021, *ApJ*, 910, 152, doi: [10.3847/1538-4357/abe40e](https://doi.org/10.3847/1538-4357/abe40e)
- Ziosi, B. M., Mapelli, M., Branchesi, M., & Tormen, G. 2014, *MNRAS*, 441, 3703